

NJC

Production of novel carbon nanostructures by electrochemical reduction of polychlorinated organic rings under mild conditions for supercapacitors

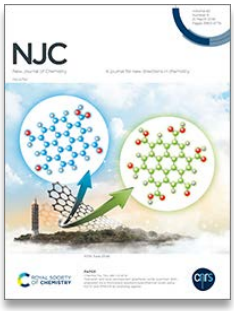
Journal:	*New Journal of Chemistry*
Manuscript ID	NJ-ART-03-2021-001542
Article Type:	Paper
Date Submitted by the Author:	29-Mar-2021
Complete List of Authors:	Kudaş, Züleyha; Atatürk University, Chemistry Çepni, Emir; Atatürk Üniversitesi Gür, Emre; Atatürk University, Physics; Ataturk Universitesi, DAYTAM Ekinci, Duygu; Ataturk, Chemistry

SCHOLARONE™
Manuscripts

NJC
New Journal of Chemistry
A journal for new directions in chemistry

Guidelines for Referees

Thank you very much for agreeing to review this manuscript for *New Journal of Chemistry*.



NJC (*New Journal of Chemistry*) is a broad-based primary journal encompassing all branches of chemistry and its sub-disciplines. It contains full research articles, communications, perspectives and focus articles.

NJC's Impact Factor is **3.288** (2019 Journal Citation Reports®)

The following manuscript has been submitted for consideration as a

PAPER

Papers report a complete study that leads to new understanding or gives new insight into the subject under investigation. If preliminary results have been published in a communication, a subsequent full paper should include additional results that justify another publication.

We ask referees to **recommend only the most significant work** for publication in *NJC*. When making your recommendation please:

- **Comment on** the originality, importance, impact and scientific reliability of the work
- **Note that routine or incremental** work should not be recommended for publication.
- **Contact the Editor** if there is any conflict of interest, if the work has been previously published or if there is a significant part of the work which you are not able to referee with confidence.

Best regards,

Contact us

Professor Jean-François Gérard
Editor-in-Chief, *NJC*

Dr Andrew Shore
Executive Editor, *NJC*

Please visit our reviewer hub for further details of our processes, policies and reviewer responsibilities as well as guidance on how to review, or click the links below.

What to do when you review

Reviewer responsibilities

Process & policies

Dr. Duygu Ekinci
Atatürk University
Faculty of Sciences
Department of Chemistry
25240 Erzurum, TURKEY
Tel : +90-442-231-4387
Fax: +90-442-236-0948
e-mail: dekin@atauni.edu.tr

March 29, 2021

Dear Dr. Gerard,

Enclosed I am submitting a manuscript entitled *"Production of Novel Carbon Nanostructures by Electrochemical Reduction of Polychlorinated Organic Rings under Mild Conditions for Supercapacitors"* to be considered for publication as a research paper in *New Journal of Chemistry*.

In this manuscript, we aimed to prepare new carbon-based nanostructures by the one-step electrochemical method using hexagonal and pentagonal polychlorinated organic rings as carbon source. For this purpose, The electrochemical growth of the carbon nanostructures on gold substrates was accomplished by electrochemical reduction of organic halides in acetonitrile solutions containing hexachlorobenzene (HCB), hexachlorocyclopentadiene (HCCP) and the mixtures of HCB and HCCP with molar ratios of 2/2, 2/1.2 and 2/0.6. The effect of HCB/HCCP molar ratio, deposition time and temperature on the morphological and structural properties of carbon coatings was investigated by various techniques. The performance of the carbon films as supercapacitors was also evaluated using cyclic voltammetry, galvanostatic charge-discharge and electrochemical impedance spectroscopy in Na_2SO_4 solution. The results showed that using a simple electrochemical reduction method, different shapes of carbon nanostructures such as nanomushrooms, nanoflowers and nanolayers could be prepared by changing the type of the precursors and the molar ratio of the precursors. Moreover, the electrochemical studies indicated that these novel carbon structures were potential candidates for supercapacitors owing to their high performance.

This article is original and unpublished and is not being considered for publication elsewhere. Therefore, we hope that this paper will be of interest to the wide.

Sincerely Yours

Dr. Duygu Ekinci

Please do not adjust margins

ARTICLE

Production of novel carbon nanostructures by electrochemical reduction of polychlorinated organic rings under mild conditions for supercapacitors

Received 00th January 20xx,
Accepted 00th January 20xx

DOI: 10.1039/x0xx00000x

Züleyha Kudaş,[a] Emir Çepni,[b] Emre Gür[c] and Duygu Ekinci*[a]

Here, new carbon-based nanostructures were prepared by the one-step electrochemical method using hexagonal and pentagonal polychlorinated organic rings as carbon source. The electrochemical growth of carbon nanostructures on substrates was accomplished by electrochemical reduction of organic halides in nonaqueous electrolyte solutions containing hexachlorobenzene (HCB), hexachlorocyclopentadiene (HCCP) and the mixtures of HCB and HCCP with molar ratios of 2/2, 2/1.2 and 2/0.6. The effect of HCB/HCCP molar ratio, deposition time and temperature on the morphological and structural properties of carbon coatings was investigated by spectroscopic and microscopic methods. The performance of carbon nanostructures as supercapacitors was also studied by cyclic voltammetry, galvanostatic charge–discharge and electrochemical impedance spectroscopy in aqueous Na_2SO_4 solution. The structural and chemical properties of carbon nanostructures was found to depend strongly on the nature and relative molar ratios of the precursors used in the electrochemical reduction process. In the case of 2/2 molar ratio of HCB to HCCP, mushroom-like carbon nanostructures are obtained, whereas, higher molar ratios of HCB to HCCP (2/1.2 and 2/0.6) result in carbon nanoflowers with graphitic feature. Furthermore, the capacitance measurements show that these novel carbon structures are potential candidates for supercapacitor-based energy storage systems because they offer high specific capacitances (332-73 F g^{-1} at 0.5 A g^{-1}), good cycling stabilities and a maximum energy density of 16 Wh kg^{-1} at a power density of 250 W kg^{-1}.

Introduction

Over the past few decades, carbon nanostructures have become one of the most attractive research areas in modern material science. Their unique electrical,[1-4] optical[5,6] and mechanical[7] properties as well as fascinating structures make them promising candidates for a variety of applications, including sensors,[8-11] fuel cells,[12-14] supercapacitors,[15,16] nano-electronics[17-19] and photonic crystals[20-22]. Since the discovery of the fullerene family in the mid of 1980s,[23] many different types of nanostructured carbon materials have been reported such as nanotubes,[24] nanoonions,[25,26] nanorings,[27] nanofibers,[28] nanohorns[29] and nanobuds[30]. The structural diversity in these materials is fundamentally determined by covalent bonding between carbon atoms and the spatial organization of carbon atoms within the structure. For instance, fullerenes are spherical carbon compounds composed of pentagonal and hexagonal faces. The most studied and well characterized fullerene is C_{60} which is commonly known as buckyball. This structure is formed by incorporation of 12 pentagonal and 20 hexagonal rings of carbon atoms. As another example, carbon nanotubes (CNTs) are carbon molecules rolled into a tube of nanometer-scale diameter. The ends of a CNT may be capped with a hemisphere of the C60 or the tube end may be open. An open-end CNT has only hexagonal rings in the structure, whereas a closed-end nanotube contains pentagonal rings in addition to hexagonal rings. A carbon nanobud is a novel carbon hybrid material synthesized via a combination of carbon nanotube and fullerene. In this material, the spherical fullerene molecules are covalently bonded to the outer sidewall of a nanotube, and thus, the nanobuds exhibit properties of both fullerenes and carbon nanotubes. Carbon onions are spherical closed carbon shells, and these structures are composed of pentagonal, hexagonal and heptagonal carbon rings. The existence of additional heptagonal rings on the outer shell improves the onion sphericity.

It is known that the shape and morphology of the nano-scale materials can be greatly influenced by the synthesis method. To date, several approaches have been developed and applied for the synthesis of carbon nanostructures, such as catalytic decomposition,[31,32] laser pyrolysis,[33] hydrothermal method,[34] and chemical vapor deposition (CVD)[35]. However, the extremely high temperature conditions (1000-4000 °C) and high operation costs of these methods limit the large-scale and low-cost production of carbon materials. Therefore, more facile and cost effective strategies for the fabrication of carbon nanostructures are urgently needed.

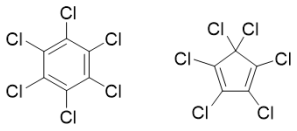
[a] Department of Chemistry, Faculty of Sciences, Atatürk University, 25240 Erzurum, Turkey.
[b] Department of Nanoscience and Nanoengineering, Nanomaterials Sciences, Atatürk University, 25240 Erzurum, Turkey.
[c] Department of Physics, Faculty of Sciences, Atatürk University, 25240 Erzurum, Turkey

† Electronic Supplementary Information (ESI) available: See DOI: 10.1039/x0xx00000x

Please do not adjust margins

We have recently shown that graphene-like carbon nanostructures could be fabricated with an electrochemical-based approach.[36] In this new procedure, we first prepared the polymer carbon films on electrodes by electroreduction of hexagonal polyhalogenated aromatic rings including hexafluorobenzene (HFB), hexachlorobenzene (HCB), and hexabromobenzene (HBB). Then, as-deposited films were exposed to thermal annealing at 400 °C to form carbon networks. The results indicate that the proposed approach is a facile and cost-effective way to produce graphene-like carbon films.

In this study, taking our goal one step further, we aim to prepare the carbon films by simultaneous electrochemical reduction of hexagonal and pentagonal polyhalogenated rings. For this purpose, various mixtures of hexachlorobenzene (HCB) and hexachlorocyclopentadiene (HCCP) (Scheme 1) were used as precursors for the electrochemical synthesis, and thus the carbon films on gold electrodes were produced. For comparison, the carbon films on electrodes were also prepared by electrochemical reduction of individual solutions of HCB and HCCP. The effect of electrolysis time, concentration ratio of polychlorinated organic compounds and temperature on morphological and chemical characteristics of carbon films was investigated by microscopic and spectroscopic methods. Also, the electrochemical capacitance properties of carbon nanostructures were studied in a three-electrode and two-electrode systems by electrochemical methods. The results showed that different types of carbon materials with high specific capacitance could be produced depending on the synthesis conditions.



Scheme 1 Structures of the hexachlorobenzene (HCB) and hexachlorocyclopentadiene (HCCP).

Results and discussion

Synthesis and characterization of carbon nanostructures

The cyclic voltammetric behaviour of HCB, HCCP and their binary mixtures was studied in anhydrous acetonitrile solution containing 0.1 M $TBABF_4$ at gold electrodes (Fig. 1). As shown in Fig. 1a, the cyclic voltammogram of HCB shows six irreversible cathodic peaks at -1.55, -1.82, -2.12, -2.38, -2.63 and -2.92 V vs. Ag/AgCl/KCl (3.0 M), which are ascribed to stepwise reductive cleavage of the six carbon-chlorine bonds.[36] On the other side, the cyclic voltammogram of HCCP exhibits a well-defined irreversible cathodic peak at -0.73 V followed by a series of small reduction peaks at -1.15, -1.47 and -1.86 V vs. Ag/AgCl/KCl (3.0 M) (Fig. 1b). This cathodic peak corresponds to the reduction of HCCP to tetrachlorocyclopentadiene (TCCP) via a concerted mechanism (a detailed study of the electrochemistry of HCCP is given in the Electronic supplementary information, Section ESI1).

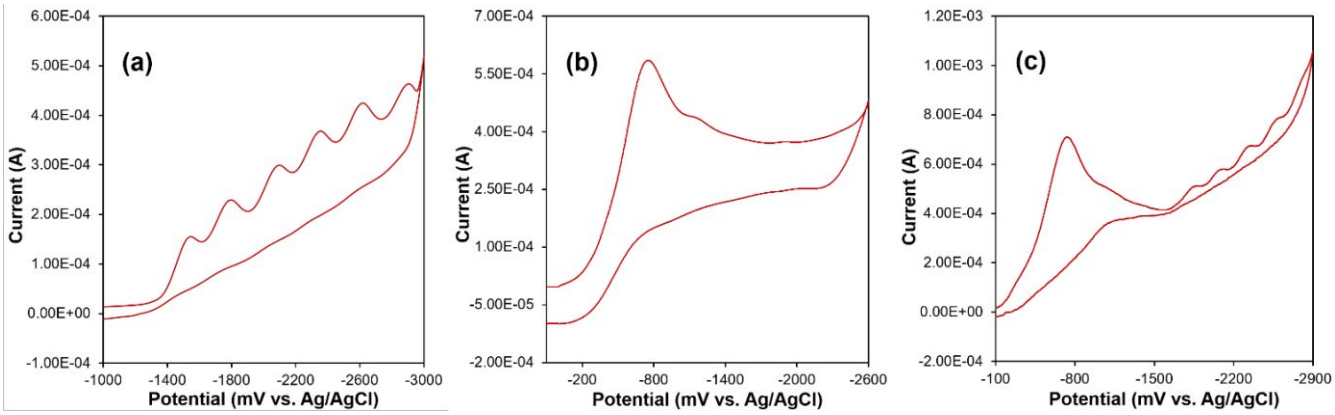


Fig. 1 Cyclic voltammetric responses of (a) HCB (2 mM), (b) HCCP (2 mM) and a mixture of HCB/HCCP (2/2) in acetonitrile containing 0.1 M $TBABF_4$ with scan rate of 0.1 V s^{-1} at gold electrodes.

After the electrochemical reduction characteristics of HCB and HCCP were examined, the cyclic voltammetric measurements of HCB and HCCP in binary mixture were carried out. Fig. 1c displays a representative cyclic voltammogram recorded in nonaqueous electrolyte solution containing HCB and HCCP with a molar ratio of 2/2. Since the polychlorinated compounds behave independently, the recorded voltammogram is the sum of each individual voltammogram with the small shifts in the peak potentials. Similar cyclic voltammograms are also obtained for the solutions containing HCB and HCCP at different molar ratios (2/1.2 and 2/0.6), except decrease in reduction peak currents of HCCP depending on its molar concentration (Fig. S5).

According to the voltammograms, electrochemical formation of carbon films on electrode surfaces by the dechlorination of both HCB and HCCP can be achieved at a higher potential than -2.8 V. Thus, potential-controlled electrolysis experiments were performed at -2.9 V vs. Ag/AgCl/KCl (3.0 M) electrode in acetonitrile solutions containing HCB, HCCP and their mixtures as a function of electrolysis

 This journal is © The Royal Society of Chemistry 20xx

time. During the electrolysis, the color of the electrolyte solutions changed from clear to brown, and the presence of black colored films on gold electrodes was observed. Then, the electrodes were taken out from electrochemical cell and were washed with acetonitrile, and the surface features of the deposited films were investigated by SEM.

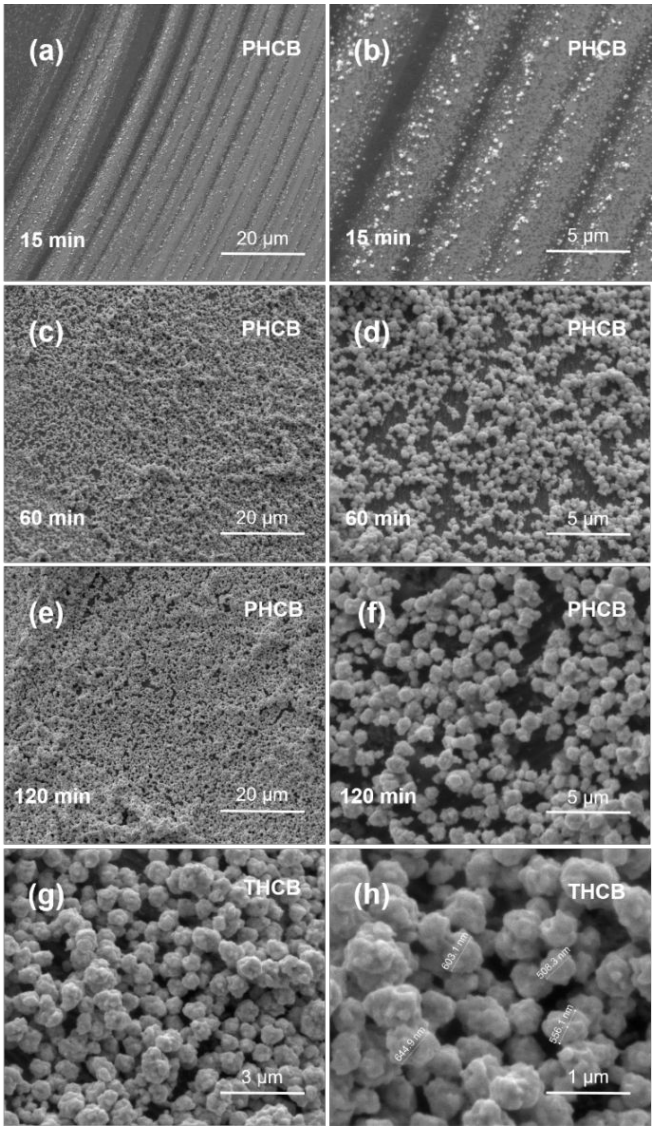


Fig. 2 SEM images of the as-deposited PHCB (a-f) and annealed THCB (g,h) films. The films were produced by potential-controlled electrolysis at -2.9 V vs. Ag/AgCl/KCl (3.0 M) at various electrolysis time (15-120 min) in acetonitrile solution containing 2 mM HCB and 0.1 M $TBABF_4$ (a-f). The PHCB film prepared after 120 min electrolysis was annealed in argon atmosphere at 400 ^{0}C for 30 min (g and h).

Fig. 2 displays the SEM images of carbon films obtained by electrochemical reduction in acetonitrile containing 2 mM HCB and 0.1 M $TBABF_4$. As can be seen from Fig. 2a and b, for a 15 min deposition time, the formation of a smooth coating with small polymer granules concentrated at the step edges of the substrate was obtained. The SEM image of the underlying smooth film closely resembles that of thin PHCB carbon film produced by potential cycling in our previous study[36]. As the electrolysis progressed (Fig. 2c and d), the thickness of electrodeposited film increased, and the granules gathered together to form the porous film. At the end of 120 min electrolysis (Fig. 2e and f), the granules changed into flower-like structure. To determine whether temperature-induced changes in the morphology, the prepared film was subjected to thermal annealing in argon atmosphere at 400 ^{0}C for 30 min. Then, the surface morphology of the annealed film was characterized by SEM (Fig. 2g and h), and no significant change was observed in the morphology and grain size (500-650 nm) of the carbon particles.

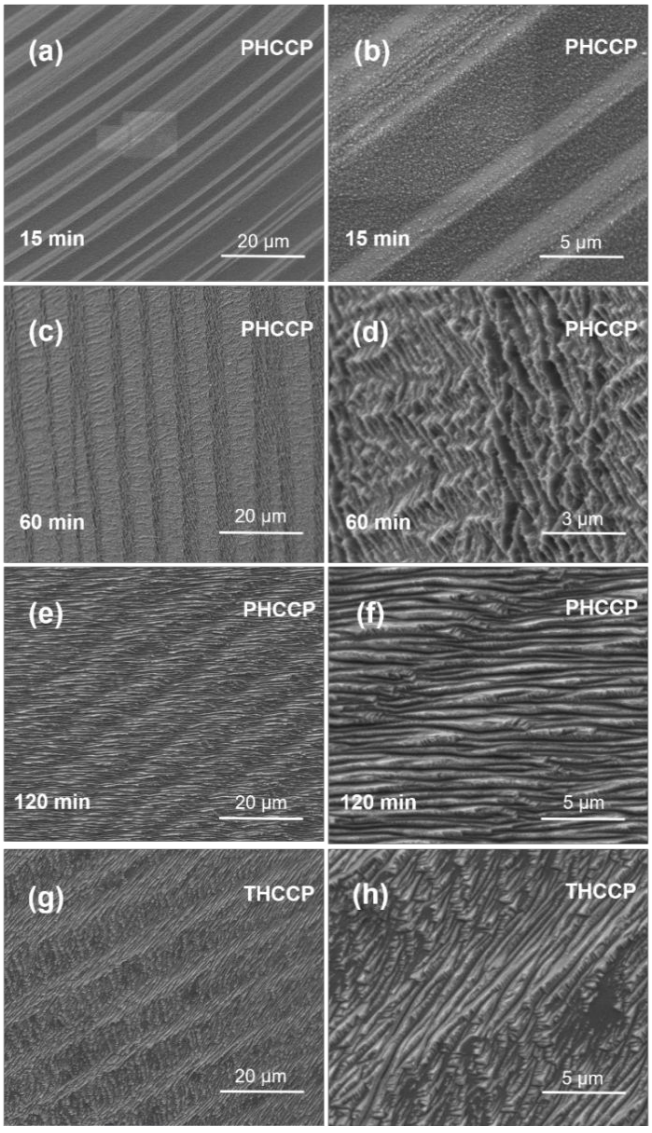


Fig. 3 SEM images of the as-deposited PHCCP (a-f) and annealed THCCP (g,h) films. The films were produced by potential-controlled electrolysis at -2.9 V vs. Ag/AgCl/KCl (3.0 M) at various electrolysis time (15-120 min) in acetonitrile solution containing 2 mM HCCP and 0.1 M $TBABF_4$ (a-f). The PHCCP film prepared after 120 min electrolysis was annealed in argon atmosphere at 400 ^{0}C for 30 min (g and h).

Fig. 3 shows the SEM images of the films electrodeposited at selected reductive potential from electrolyte solution containing 2

mM HCCP. At the beginning of the electroreduction (Fig. 3a and b), the whole surface of the electrode was covered with a more smooth polymer film. As the deposition time increases, the film revealed a laminar structure of oriented carbon layers (Fig. 3c and d). After 120 min, the long and smooth paths with obvious boundaries were observed all over the surface (Fig. 3e and f). Moreover, after thermal annealing, the annealed film retained the same morphology (Fig. 3g and h).

Fig. S6-S8 show the SEM images of the carbon nanostructures formed on gold electrodes via electrochemical reduction in binary mixture solutions containing different molar ratios of HCB and HCCP (2/0.6, 2/1.2 and 2/2), whereas Fig. 4 displays the SEM images of these films after annealing at 400 ^{0}C for 30 min. The images clearly show that when the amount of the HCCP is low (0.6 mM), the irregularly-shaped and non-uniform particles are formed with increasing electrolysis time (Fig. S6). Furthermore, when the resulting structures were annealed at 400 ^{0}C, they became more irregular and slacker (Fig. 4a and b). As the concentration of HCCP increases to a medium level (1.2 mM), the growth of nanoflower-like carbon particles with different sizes was obtained (Fig. S7). Also, the annealing process at 400 ^{0}C promoted formation of larger and more homogeneous geometries with realignment of carbon particles (Fig. 4c and d). The change in concentration of HCCP from 1.2 mM to 2 mM caused a drastic change in the morphology of the resulting material. In this case, as seen in Fig. S8, novel mushroom-like carbon nanostructures were formed on gold electrode. Also, after thermal treatment of the film at 400 ^{0}C, the structures maintained their mushroom-like nature (Fig. 4e and f).

To explore the growth process of mushroom-like carbon nanostructures, the carbon films on gold electrodes were accomplished by potential cycling between -0.1 V and -2.9 V vs. Ag/AgCl/KCl (3.0 M) at a scan rate of 0.1 V s^{-1} in 0.1 M $TBABF_4$/acetonitrile solution containing 2 mM HCB and 2 mM HCCP. After completing 50 cycles, the electrode was taken out from electrochemical cell and then characterized by SEM (Fig. S9a and b). The deposit film was found to contain spherical mushroom cap-shaped and mushroom stem-shaped particles as well as several partially formed mushroom-like carbon structures. After the second 50 cycles, it was obtained that most of the particles were converted mushroom-like structures (Fig. S9c).

To identify the elemental composition of the resulting carbon films deposited by 120 min electrolysis before and after annealing at 400 ^{0}C, the XPS C1s and Cl2p energy regions of the films were analyzed. Fig. 5 displays the fitted XPS spectra of the C1s region for the films. As shown, the fitting of this region for all samples reveals three components at about 284, 285 and 287 eV. The peak with the lowest binding energy around 284 eV originates from the sp^2-hybridized carbons, while the peak located at 285 eV corresponds to the sp^3-hybridized carbon atoms[37]. The peak at about 287 eV is also due to carbon atoms linked to chlorine atoms. For all carbon films, after annealing at 400 ^{0}C, the atomic percent for sp^2-hybridized carbon atoms increases whereas the atomic percent of carbon atoms linked to halogen atom decreases (Table S1). As expected, the highest atomic percent of sp^2- and sp^3-hybridized carbon atoms was

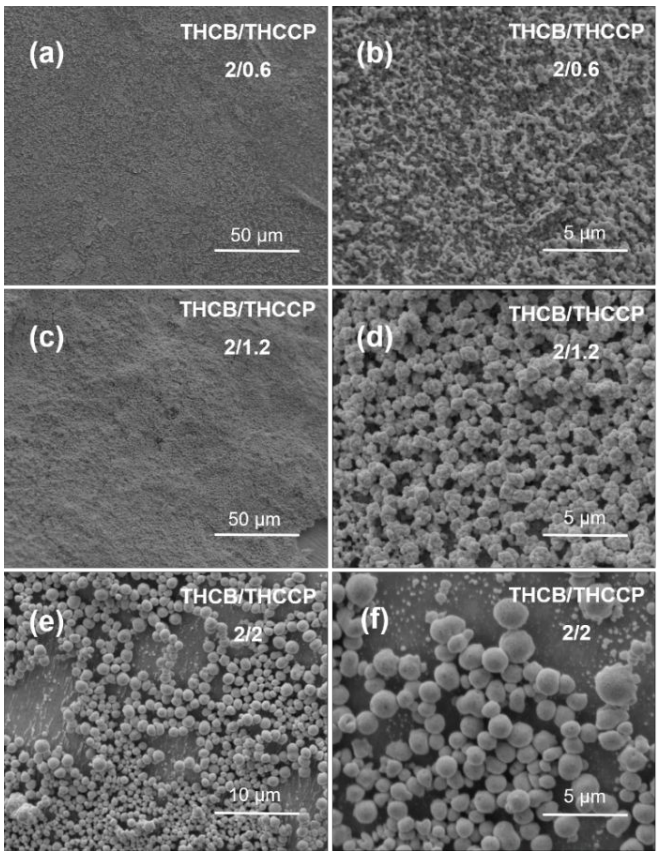


Fig. 4 SEM images recorded after annealing for the carbon films obtained by potential-controlled electrolysis (120 min) in 0.1 M $TBABF_4$/acetonitrile solution containing different molar concentrations of HCB and HCCP.

observed for THCB and PHCCP films, respectively. Also, after annealing, the atomic percent of sp^3-hybridized carbon atoms increased for the THCB/THCCP:2/0.6 sample, indicating that the defect density in the structure increased through an annealing heat treatment. This result was also confirmed by SEM analysis in which the film became more disordered (Fig. 4a and b). On the other hand, it was observed that the higher molar concentration of HCCP in electrolyte solution caused an increase of atomic percent of sp^2-hybridized carbon atoms. This result can be explained by participation of pentagonal HCCP molecules in carbon structures, and thus by the formation of the curved structures on the caps of mushroom-like structures for the PHCB/PHCCP:2/2 and TCB/THCCP:2/2 films (Fig. S8, Fig. S9 and Fig. 4e and f).

The results of the curve fit analysis of the XPS Cl2p region are shown in Fig. S10. All spectra, except those of PHCB and THCB, reveal the presence of three sets of spin-orbit doublets of $Cl2p_{3/2}$ and $Cl2p_{1/2}$ originating from three different chlorine atoms. These peaks can be attributed to chlorine atoms bonded to sp^2-hybridized carbon atoms (202-200 eV), chlorine atoms bonded to sp^3-hybridized carbon atoms (200-198 eV) and chlorine atoms belonging to CCl_2 on HCCP ring (198-196 eV), respectively[37]. As seen, after annealing at 400 ^{0}C, the atomic percent for chlorine atoms belonging to CCl_2 decreases for the films (Table S2). On the other hand, after annealing, the atomic percent of chlorine atoms bonded to sp^3-hybridized carbons

 This journal is © The Royal Society of Chemistry 20xx

Please do not adjust margins

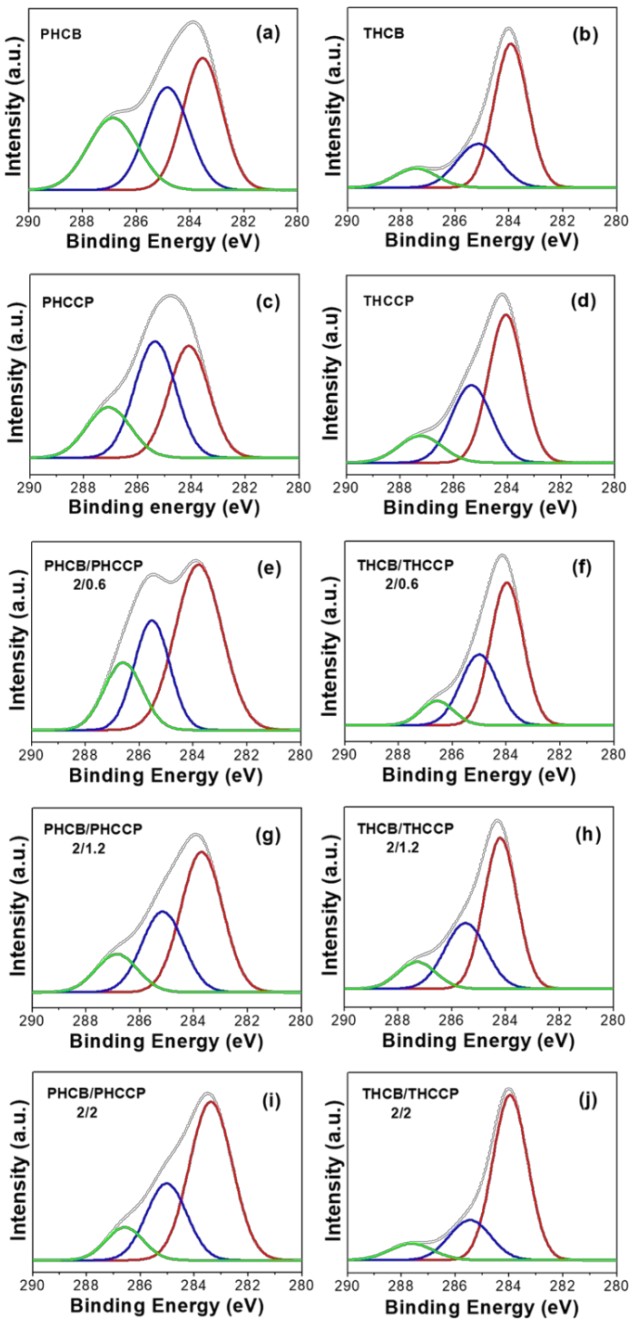


Fig. 5 Deconvoluted C1s XPS spectra of carbon films deposited by 120 min electrolysis before and after annealing at 400 ^{0}C.

increases for the THCB/THCCP:2/0.6 and THCB/THCCP:2/1.2 samples, whereas the atomic percent of chlorine atoms bonded to sp^3-hybridized carbons decreases for the THCB/THCCP:2/2 sample.

In order to gain further insight into the chemical characteristics of the films, additional spectroscopic analysis was carried out by Raman technique. The Raman spectra were recorded in the 800-2000 cm^{-1} range since this spectral region provides useful structural information about carbon materials[38]. Fig. 6 shows the deconvoluted Raman spectra of as-deposited and annealed carbon films prepared with electrochemical reduction using HCB and HCCP precursors. As seen in Fig. 6a, the deconvoluted spectrum of PHCB film reveals the presence of seven components. The peak around 1569 cm^{-1}, commonly known as the G band, is related to the in-plane stretching-vibration of sp^2 sites in olefinic chains and/or aromatic rings. The peak at about 1340 cm^{-1} (D1-band) corresponds to the breathing mode of sp^2 sites in disordered hexagonal ring structure. The spectrum depicts a peak at 1623 cm^{-1} (D2) observed as shoulder on the G band, indicating the presence of disordered sp^2 structures[39]. Another peak is also observed at 1432 cm^{-1} (D3), which is associated with amorphous sp^2-bonded forms of carbon[40,41]. Furthermore, the Raman spectrum reveals weak peaks at 1289, 1234 and 1127 cm^{-1} (D4 bands). The origin of these peaks is still unclear, however, it is suggested that they might originate from different kinds of carbon such as amorphous sp^3-carbon, amorphous mixed sp^2/sp^3-carbon and hydrogenated-like carbon[42].

After annealing at 400 ^{0}C, the Raman spectrum of THCB film revealed the presence of similar characteristic peaks with the exception of relatively minor shifts in all peak positions and splitting of the D3 band at 1432 cm^{-1} into two distinct sub-bands (Fig. 6b and Table S3). The seven Raman modes related to carbon structures were also observed in the fitted spectra of PHCCP and THCCP (Fig. 6c and d) in which two dominant D and G bands were at higher frequencies in comparison to those of PHCB and THCB (Table S3).

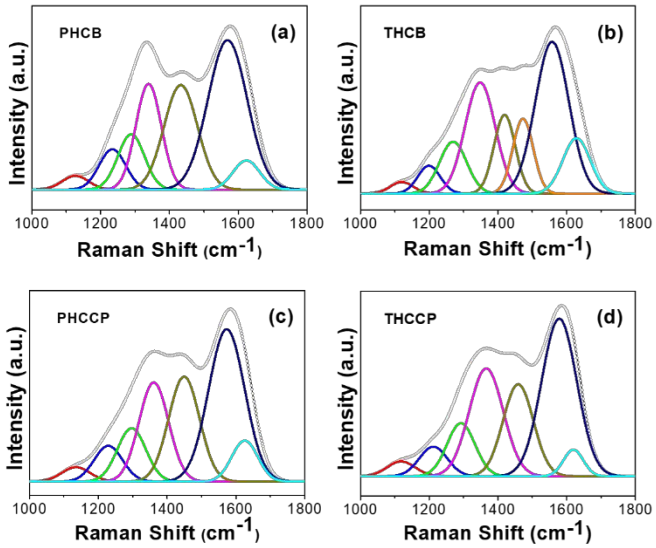


Fig. 6 Deconvoluted Raman spectra of carbon films deposited by potential-controlled electrolysis in 0.1 M $TBABF_4$/acetonitrile solution containing HCB and HCCP before and after annealing at 400 ^{0}C.

Similar results were obtained for thermal-annealed carbon films after electrochemical deposition in binary mixture solutions containing different molar ratios of HCB and HCCP (Fig. 7). The fitted Raman spectra showed that the G band positions were ranged from 1562 cm^{-1} to 1574 cm^{-1} and that this band position was shifted to higher frequencies with increasing amount of HCCP in electrolyte solution (Table S3). Also, it was obtained that the peaks between 1000 and 1300 cm^{-1} were shifted toward the lower frequencies compared to those of THCB and THCCP films (Table S3).

This journal is © The Royal Society of Chemistry 20xx

Please do not adjust margins

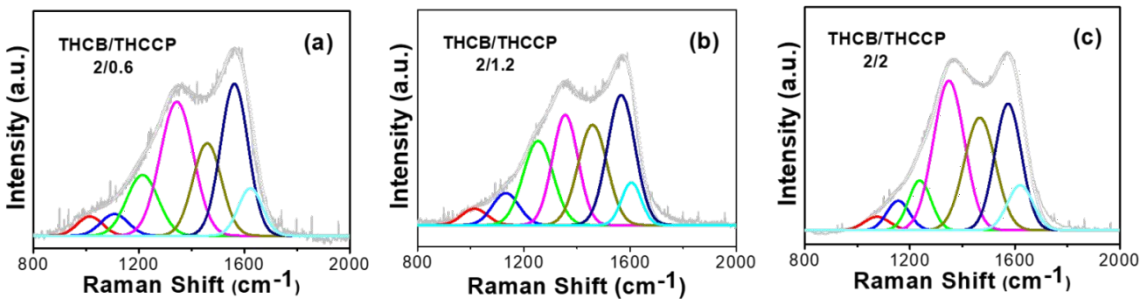


Fig. 7 Deconvoluted Raman spectra of carbon films deposited by potential-controlled electrolysis in 0.1 M $TBABF_4$/acetonitrile solution containing different molar ratios of HCB and HCCP after annealing at 400 ^{0}C.

Electrochemical performance of carbon nanostructures

The electrochemical performance of carbon films as active electrode materials in electrochemical capacitors was first evaluated in a three-electrode configuration with 1 M Na_2SO_4 aqueous electrolyte solution. The cyclic voltammetry (CV), galvanostatic charge-discharge (GCD) and electrochemical impedance spectroscopy (EIS) techniques were used to investigate the samples. The applied potential was varied in the range of 0.0 V and +0.8 V vs. Ag/AgCl/KCl (3.0 M) reference electrode. Fig. 8a shows the CV curves of the PHCB/Au, THCB/Au, PHCCP/Au and THCCP/Au electrodes at a scan rate of 100 mV s^{-1}. The curves of the PHCB, THCB and THCCP films exhibit nearly rectangular shapes, however, the cyclic voltammogram of the PHCCP film shows broad and weak redox peaks around +0.2 V and +0.6 V vs. Ag/AgCl/KCl (3.0 M) reference electrode. The presence of redox peaks in the CV indicates that the energy storage in the PHCCP film can be achieved by means of both electrostatic and pseudocapacitive charging. This behavior has been observed for various carbon materials containing surface functional groups such as hydroxyl, carbonyl and amine[43].

The specific capacitances ($C_{s,CV}$) were calculated from the CV curves using the following equation,

$$C_{s,CV} = \frac{\int I(V)dV}{m \times \Delta V \times \nu}$$

where $C_{s,CV}$ (F g^{-1}) is the specific capacitance obtained from CVs, I (A) is the capacitive current, m (g) is the mass of the active material, ΔV (V) is the potential range and ν (V s^{-1}) is the scan rate.

At the same scan rate of 100 mV s^{-1}, the specific capacitance values for the PHCCP/Au and THCCP/Au electrodes were found to be 196.6 and 209.2 F g^{-1}, respectively. These values are much higher than those of the PHCB (110.7 F g^{-1}) and THCB (80.2 F g^{-1}) electrodes (Table S4). This result suggests that the laminar orientation of the carbon layers allows easy diffusion of the electrolyte ions into the electrode/electrolyte interface, and thus provides higher electrochemical activity. Besides, the prominent electrochemical behavior of PHCCP film can be ascribed to the contribution of pseudocapacitance as well as the double-layer capacitance to the overall measured capacitance value. On the other hand, the capacitances of the films annealed at 400 ^{0}C (THCB and THCCP) are generally lower than those of the as-prepared carbon films (PHCB and PHCCP), indicating that the removal of surface chlorine atoms results in reduced capacitances.

Fig. S11 demonstrates the CV curves of the carbon films at different scan rates (20-500 mV s^{-1}). As seen, the specific capacitance values gradually decreased with increasing scan rate (Fig. 8b, Table S4), since the electrolyte ions have sufficient time to penetrate into the films at low scan rates[44].

The capacitive performance of the films was further investigated by galvanostatic charge-discharge experiments. Fig. 8c shows a comparison of GCD curves for PHCB/Au, THCB/Au, PHCCP/Au and THCCP/Au electrodes at a constant current density of 0.5 A g^{-1}, whereas Fig. S12 displays the corresponding GCD curves for the electrodes under different current densities of 0.5, 1, 3, 5, 7, 10 and 20 A g^{-1}. The average specific capacitance values ($C_{s,GCD}$) of the electrodes were determined from the GCD values according to the following equation,

$$C_{s,GCD} = \frac{I \times \Delta t}{m \times \Delta V}$$

where $C_{s,GCD}$ (F g^{-1}) is the specific capacitance obtained from GCDs, I (A) is the applied current density, Δt (s) is the discharge time, m (g) is the total mass of the active materials, ΔV (V) is the potential range of the charge and discharge.

The charge-discharge capacitances of the PHCCP/Au and THCCP/Au electrodes are much higher than those of the PHCB/Au and THCB/Au electrodes (Table S4), which supports the experimental results obtained from CV measurements. Also, the specific capacitance values gradually decreased as the current density increases from 0.5 to 20 A g^{-1}.

To further understand the conductivity and charge storage performances of the samples, EIS measurements were performed in the frequency range from 0.1 MHz to 10 Hz. Fig. 8d shows the Nyquist plots of the PHCB/Au, THCB/Au, PHCCP/Au and THCCP/Au electrodes in Na_2SO_4 (1 M) electrolyte solution. The experimental data were fitted using the equivalent electrical model shown in the inset of Fig. 8d, where the R_s is the equivalent series resistance, C_{dl} is the double capacitance, CPE is the constant phase element, R_{ct} is the charge transfer resistance and Z_W is the Warburg impedance[45,46]. In the high frequency region, the intercept on the real axis corresponds R_s which is an incorporation of the diffusion resistance of the electrolyte ions,

 This journal is © The Royal Society of Chemistry 20xx

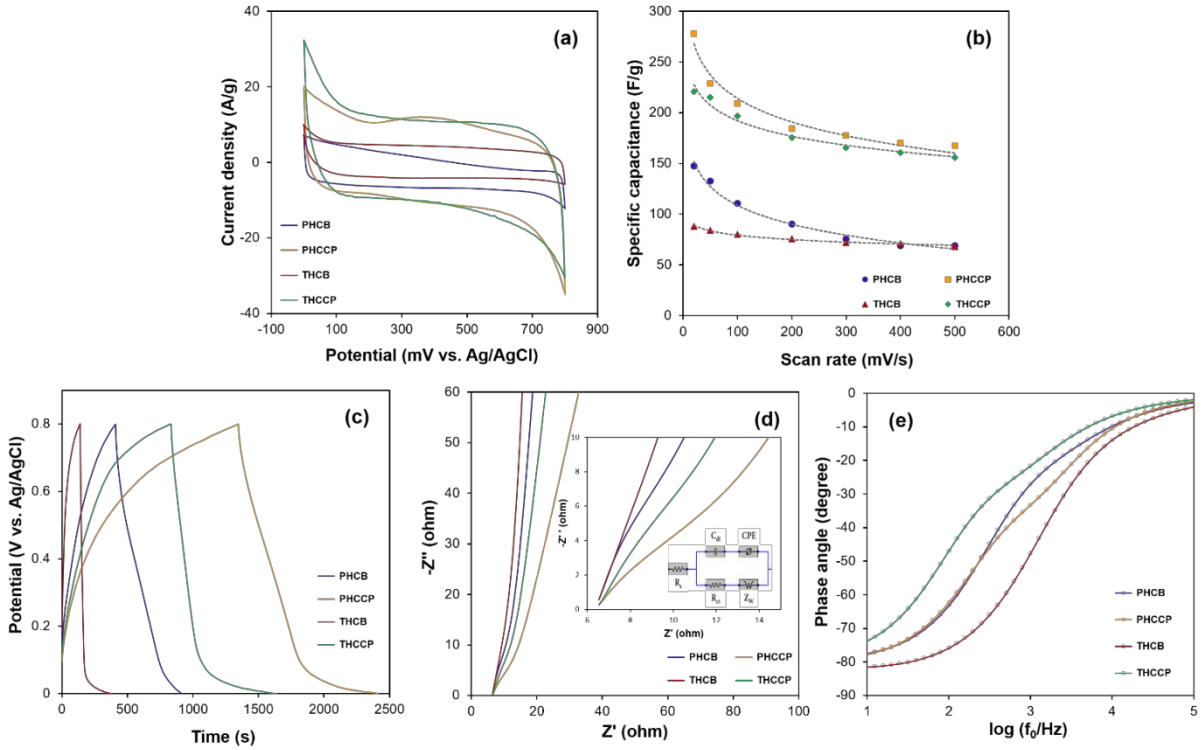


Fig. 8 Electrochemical performances of the carbon films using a three electrode system cell in 1 M Na_2SO_4 aqueous solution. (a) CV curves recorded on PHCB/Au, THCB/Au, PHCCP/Au and THCCP/Au electrodes at 100 mV s^{-1}. (b) Plots of the specific capacitances versus scan rate for the carbon films on Au electrodes. (c) GCD curves of the PHCB/Au, THCB/Au, PHCCP/Au and THCCP/Au electrodes at a current density of 0.5 A g^{-1}. (d) Nyquist diagrams of the PHCB/Au, THCB/Au, PHCCP/Au and THCCP/Au electrodes in the frequency range from 0.1 MHz to 10 Hz. The insets show enlargement of the high frequency region and the equivalent circuit to fit experimental results. (e) Bode plots of the PHCB/Au, THCB/Au, PHCCP/Au and THCCP/Au electrodes.

the intrinsic resistance of active electrode material, and the contact resistance between the current collector and carbon materials. R_{ct}, the charge transfer resistance for the redox reactions at the electrode/electrolyte interface, which is related to the diameter of the semicircle. In the low frequency region, the straight line is correlated with the Z_W, which shows the diffusion rate of the electrolyte ions into carbon materials. The more vertical line suggests efficient diffusion of electrolyte ions to the active material. As shown in Fig. 8d and in the inset of Fig. 8d, the curves exhibit a nearly straight line with a very small depressed semicircle. This result indicates that all the films have good conductivity and low diffusion and charge transfer resistance (Table S5). Fig. 8e shows the Bode plots of the frequency responses. The characteristic frequencies (f_0) for a phase angle of -45^0 of the PHCB/Au, THCB/Au, PHCCP/Au and THCCP/Au electrodes are 330, 114, 400 and 124 Hz, respectively. The corresponding relaxation time constants (T_0=1/f_0) are 3.0 ms (PHCB/Au), 8.8 ms (THCB/Au), 2.5 ms (PHCCP/Au) and 8.1 ms (THCCP/Au) (Table S5). The small time constants of the electrodes further confirm the fast ion diffusion in carbon films as supercapacitor electrodes[47,48].

Fig. 9a and b show comparative CV curves of the PHCB/PHCCP/Au and THCB/THCCP/Au electrodes obtained by electrochemical reduction in binary mixture solutions containing different molar ratios of HCB and HCCP (2/0.6, 2/1.2, and 2/2). The voltammograms were recorded in 1 M Na_2SO_4 solution at a scan rate of 100 mV s^{-1}, and the specific capacitance of each electrode was determined from the voltammograms (Table S4). The values are in the range of 80-250 F g^{-1}, and the PHCB/PHCCP:2/2 (218.1 F g^{-1}) and THCB/THCCP:2/2 (251.0 F g^{-1}) films exhibit higher specific capacitances than those of other carbon films. Also, the specific capacitances of the films decrease with the increasing scan rates (Fig. 9c and Fig. S13).

The cycling capabilities of the films were investigated for 1000 voltammetric cycles at a scan rate of 100 mV s^{-1} because long cycling stability is a crucial factor for practical supercapacitor applications. As seen in Fig. 9d and e, the PHCB/PHCCP:2/2 film retains 84.6% of the initial capacitance after 1000 cycles, however, the THCB/THCCP:2/2 film exhibits a serious capacitance degradation of 49.4% after 1000 cycles.

The supercapacitive properties of the electrodes were also evaluated by the GCD measurements, and the specific capacitances were obtained according to the GCD curves. Typical GCD responses recorded for the electrodes at the current density of 0.5 A g^{-1} are shown in Fig. 9f and g. The PHCB/PHCCP:2/2 and THCB/THCCP:2/2

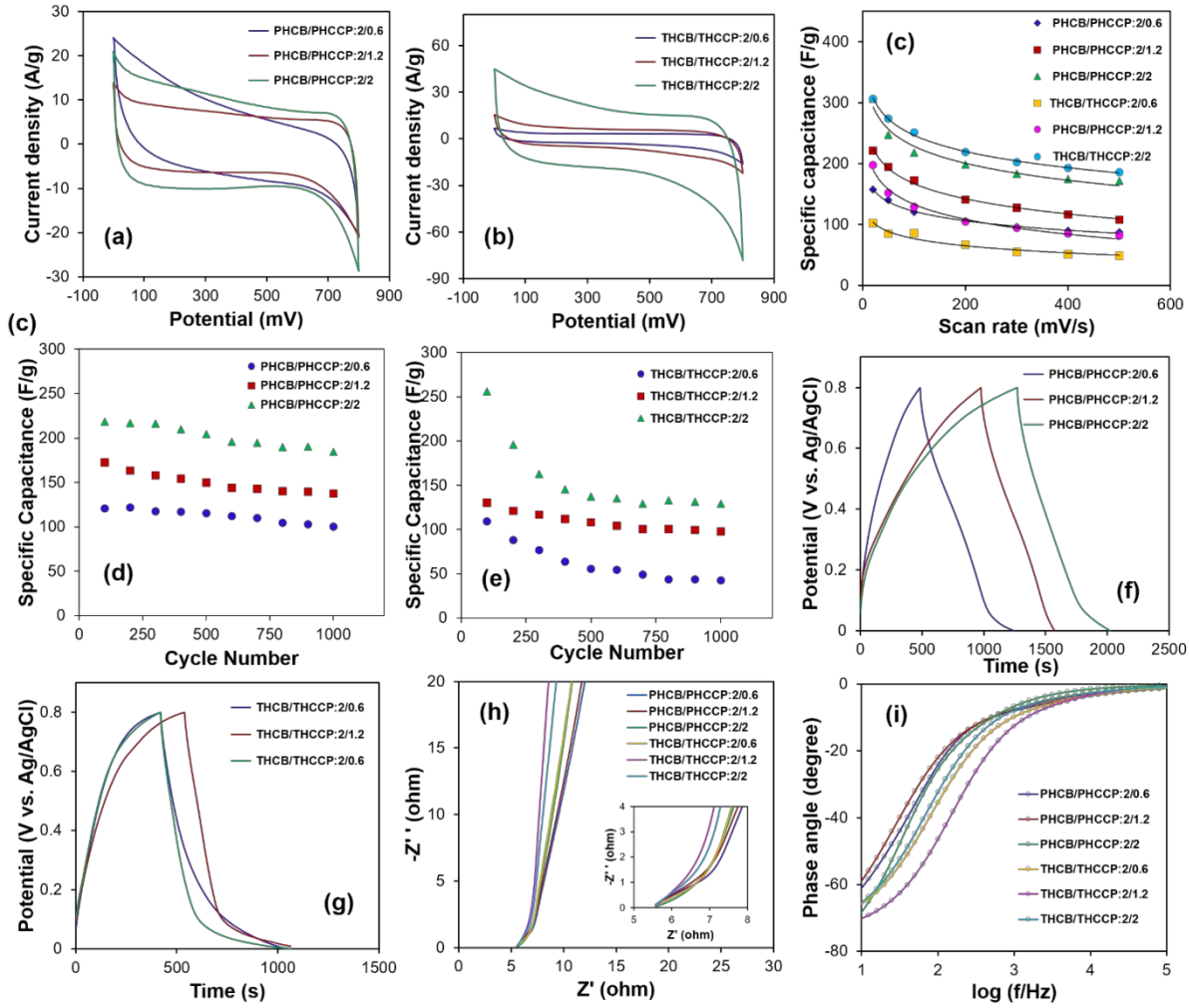


Fig. 9 Electrochemical performances of the carbon films using a three electrode system cell in 1 M Na_2SO_4 aqueous solution. (a) CV curves recorded for PHCB/PHCCP:2/0.6, PHCB/PHCCP:2/1.2 and PHCB/PHCCP:2/2 films at 100 mV s^{-1}. (b) CV curves recorded for THCB/THCCP:2/0.6, THCB/THCCP:2/1.2 and THCB/THCCP:2/2 films at 100 mV s^{-1}. (c) Plots of the specific capacitances versus scan rate for the carbon films on Au electrodes. (d) Variation of specific capacitances with cycle number for PHCB/PHCCP:2/0.6, PHCB/PHCCP:2/1.2 and PHCB/PHCCP:2/2 films. (e) Variation of specific capacitances with cycle number for THCB/THCCP:2/0.6, THCB/THCCP:2/1.2 and THCB/THCCP:2/2 films. (f) GCD curves of the PHCB/PHCCP:2/0.6, PHCB/PHCCP:2/1.2 and PHCB/PHCCP:2/2 films at a current density of 0.5 A g^{-1}. (g) GCD curves of the THCB/THCCP:2/0.6, THCB/THCCP:2/1.2 and THCB/THCCP:2/2 films at a current density of 0.5 A g^{-1}. (h) Nyquist diagrams of the carbon films in the frequency range from 0.1 MHz to 10 Hz. Inset shows enlargement of the high frequency region and the equivalent circuit model. (i) Bode plots of the carbon films on Au electrodes.

films exhibit the specific capacitances of 235 and 201 F g^{-1} at a current density of 0.5 A g^{-1}, respectively, which are larger than those of the carbon films prepared at lower molar concentrations of HCCP. On the other hand, the specific capacitances of the films decrease with an increase in the current density (Fig. S14 and Table S4).

The characteristics of supercapacitors strongly depends on the physical/chemical properties of active material, including surface morphology, surface area, pore size distribution and electrical conductivity[49,50]. In this regard, the surface area and porosity characteristics of the carbon films before annealing at 400 ^{0}C were obtained by the Brunauer-Emmett-Teller (BET) and Barrett-Joyner-Halenda (BJH) method. The results show that the PHCB/PHCCP:2/2 has a higher specific surface area (1955 m^2 g^{-1}) than that of the PHCB/PHCCP:2/0.6 and PHCB/PHCCP:2/1.2 films (1242 and 1454 m^2 g^{-1}, respectively) (Table S6). Accordingly, the higher capacitance of PHCB/PHCCP:2/2 may be due to the larger specific surface area of mushroom-like structure, increasing the amount of adsorption/desorption sites of the PHCB/PHCCP:2/2 film for the ion diffusion during the charge-discharge process.

The ion and electron transfer performances of the films were examined by EIS measurements (Fig 9h), and the impedance spectra of the samples were fitted to the same equivalent circuit model (inset of Fig. 8d). The fitted data for circuit elements are given in Table S5. As seen, all the samples possess small R_s, R_{ct} and Z_w values, indicating

This journal is © The Royal Society of Chemistry 20xx

Please do not adjust margins

ideal capacitance behaviors of the electrode materials. Also, as observed in the impedance Bode plots (Fig. 9i), the small relaxation time constants (T_0) indicate that the carbon films are suitable electrode materials for supercapacitor applications (Table S5).

To explore the practical applications of the obtained carbon materials in supercapacitors, solid-state symmetric supercapacitor devices were prepared and electrochemically tested in 1 M Na_2SO_4. THCB/THCCP:2/0.6, THCB/THCCP:2/1.2 and THCB/THCCP:2/2 carbon nanostructures were the active electrode materials used in supercapacitor devices. Fig. 10a-c shows the measured CV curves in the two-electrode system under a potential window of 0.0 V and +1.0 V vs. Ag/AgCl/KCl (3.0 M) at various scan rates (20-500 mV s^{-1}). As seen, the CV curves for THCB/THCCP:2/2 device exhibit a more rectangular shape and larger area than that of the other devices (Fig. 10c), which indicates that THCB/THCCP:2/2 has the best capacitive performance. The GCD curves of the symmetric capacitors at current densities 0.5 to 10 A g^{-1} are shown in Fig. 10d-f. In the two-electrode system, the specific capacitances of the capacitors ($C_{s,CELL}$, F g^{-1}) were calculated from the discharge profile of the GCD measurements using the following equation,

$$C_{s,CELL} = \frac{I \times \Delta t}{m_t \times \Delta V}$$

where I (A) is the discharge current, Δt (s) is the discharge time, m_t (g) is the total mass of active materials on the two current collectors of the device and ΔV (V) is the potential window. According to this equation, the specific capacitances of the THCB/THCCP:2/0.6, THCB/THCCP:2/1.2 and THCB/THCCP:2/2 at a current density of 0.5 A g^{-1} were obtained as 36.3, 88.8 and 116.1 F g^{-1}, respectively. With the increase of current density from 0.5 A g^{-1} to 10 A g^{-1}, 37.4%, 11.8% and 23.4% of the initial capacitances are retained for THCB/THCCP:2/0.6, THCB/THCCP:2/1.2 and THCB/THCCP:2/2, respectively (Table S7).

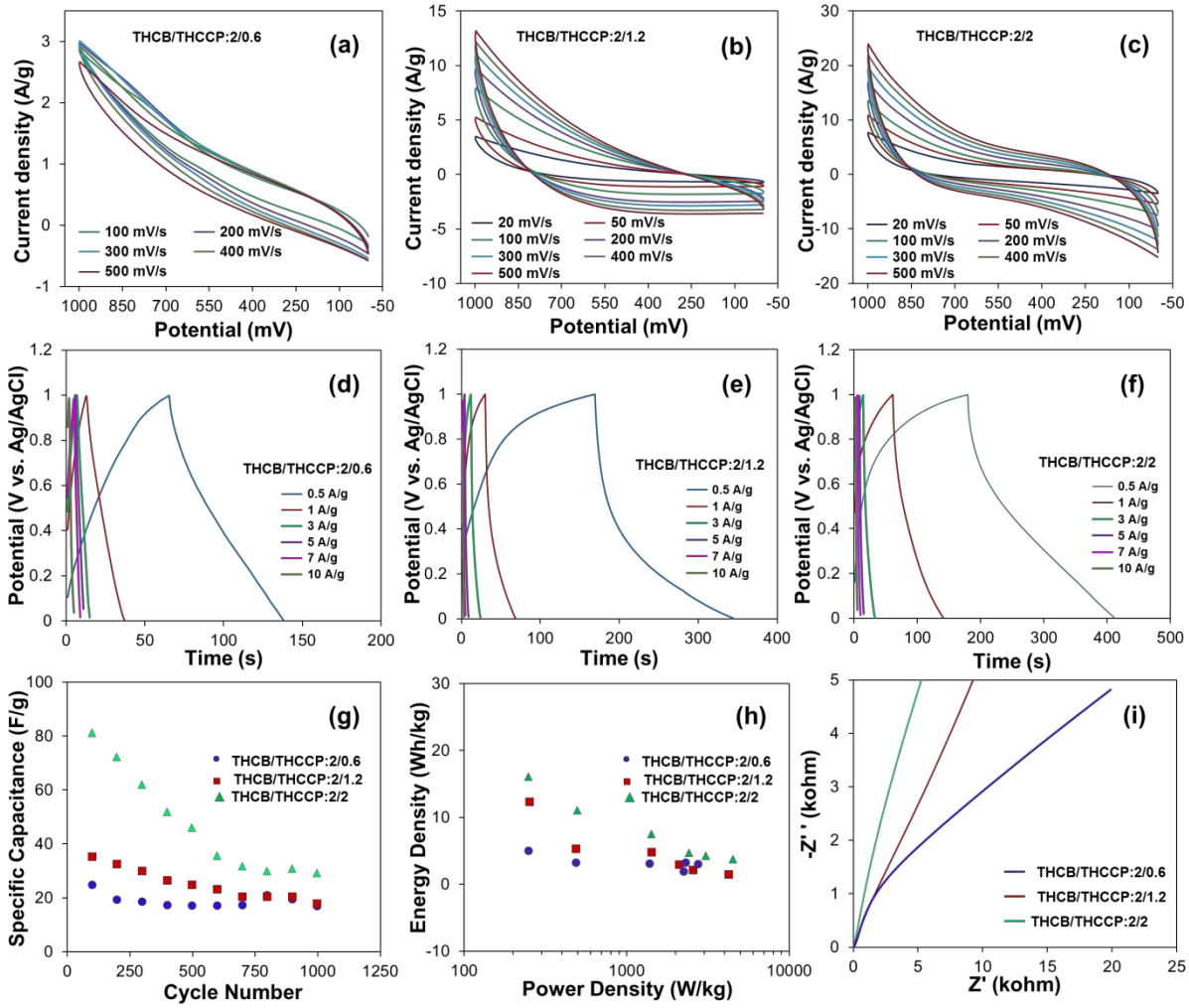


Fig. 10 Electrochemical performances of the symmetric supercapacitors under the two-electrode system. CV curves of (a) THCB/THCCP:2/0.6, (b) THCB/THCCP:2/1.2 and (c) THCB/THCCP:2/2 electrodes at different scan rates. GCD curves of (d) THCB/THCCP:2/0.6, (e) THCB/THCCP:2/1.2 and (f) THCB/THCCP:2/2 electrodes at different current densities. For THCB/THCCP:2/0.6, THCB/THCCP:2/1.2 and THCB/THCCP:2/2 electrodes (g) variation of specific capacitances with cycle number, (h) Ragone plot and (i) Nyquist diagrams in the frequency range from 0.1 MHz to 10 Hz.

In order to evaluate the long-term stability of the symmetric supercapacitors, CV scans within 0.0 V and +1.0 V voltage range (vs. Ag/AgCl/KCl (3.0 M)) were performed with the scan rate of 100 mV s^{-1} (Fig. 10g). After 1000 cycles, the THCB/THCCP:2/1.2 and THCB/THCCP:2/0.6 devices display the cycle lifetimes with retention of 50.6% and 68.2% of their initial measured values, respectively. By contrast, the THCB/THCCP:2/2 possesses the capacitance retention of 35.9%. This severe decrease in the capacitance for the THCB/THCCP:2/2 carbon structures is also obtained with electrochemical measurements performed by using three electrode system (Fig. 9e).

Based on the GCD profiles, the energy density (E, Wh kg^{-1}) and power density (P, W kg^{-1}) of the symmetric devices were calculated according to the following equations[51,52],

$$\mathrm{E} = \frac{\mathrm{C_{s,CELL}} \times \Delta V^2}{2 \times 3.6} \quad and \quad \mathrm{P} = \frac{\mathrm{E} \times 3600}{\Delta \mathrm{t}}$$

where $C_{s,CELL}$ (F g^{-1}) is the specific capacitance of the symmetric supercapacitor, ΔV (V) is the voltage window of discharge curve and Δt (s) is the discharge time. The results obtained are summarized in a Ragone plot (Fig. 10h). The THCB/THCCP:2/2 symmetric device shows the highest energy density of 16.1 Wh kg^{-1} under the power density 250.1 W kg^{-1} and highest power density of 4524 W kg^{-1} with energy density of 3.8 Wh kg^{-1}. On the other hand, the THCB/THCCP:2/0.6 device presents a maximum energy density of 5.1 Wh kg^{-1} and a maximum power density of 2754 W kg^{-1}. The obtained energy and power densities are comparable to previously reported carbon-based symmetric supercapacitors, including porous graphene/carbon cloth (1.64 Wh kg^{-1} at 670 W kg^{-1})[53], porous carbon/graphene composite (10.1 Wh kg^{-1} at 7.26 kW kg^{-1})[54], biopolymer derived porous graphitic carbon (13.5 Wh kg^{-1} at 777 W kg^{-1})[55], nitrogen-doped carbon nanofibers (5.9 Wh kg^{-1} at 1.2 kW kg^{-1})[56], nitrogen-doped bio-oil derived carbon (8.91 Wh kg^{-1} at 253.8 W kg^{-1})[57] and oxygen/nitrogen-doped biomass derived carbon (20 Wh kg^{-1} at 178.6 W kg^{-1})[58].

The capacitive behavior of the symmetric capacitors was also investigated by EIS measurements (Fig. 10i), and the impedance spectra of the devices were fitted to the equivalent electrical circuit shown in the inset of Fig. 8d. Among the devices, the THCB/THCCP:2/0.6 capacitor displays a less steep vertical straight line in the low frequency region. This result indicates that the THCB/THCCP:2/0.6 capacitor has lower capacitive characteristic than those of the THCB/THCCP:2/2 and THCB/THCCP:2/1.2 devices, which are consistent with the CV and GCD data.

Fig. 11 shows that two THCB/THCCP:2/2 symmetric supercapacitors can easily light a red commercial light emitting diodes (LEDs) for ~12 min. Similar phenomena are also obtained for the THCB/THCCP:2/1.2 and THCB/THCCP:2/0.6 devices with the shorter time periods. These observations demonstrate the great potential of carbon nanostructures for practical applications.

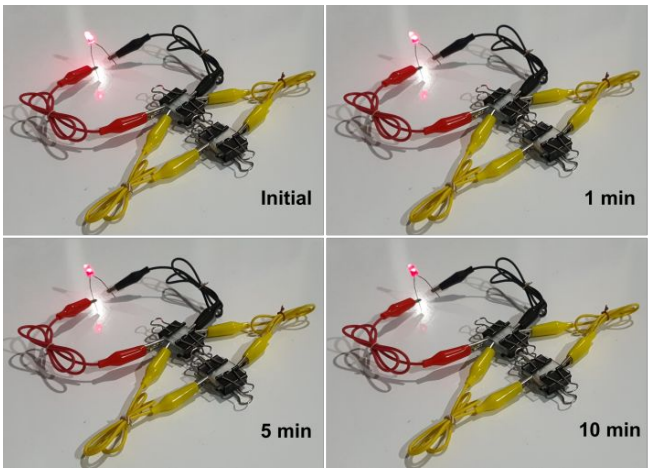


Fig. 11 The application of THCB/THCCP:2/2 symmetric supercapacitor.

Experimental

Materials and chemicals

Hexachlorobenzene (HCB), hexachlorocyclopentadiene (HCCP) and other chemicals were purchased from Sigma-Aldrich and used as received. Au wire (0.762 mm diameter, 99.999% purity) and Au foil (0.127 mm diameter, 99.99% purity) were obtained from Alfa Aesar. Acetonitrile was purified by distillation over calcium hydride. Tetrabutylammonium tetrafluoroborate ($TBABF_4$) was purified by recrystallization. Aqueous solutions were prepared with deionized water (18 MΩ cm^{-1}) from a Barnstead Nanopure water purification system.

Preparation of carbon films

The cyclic voltammetric studies were conducted on a Bioanalytical Systems BAS-100B electrochemical analyzer in a three-electrode configuration. A platinum wire (BAS Model MW-1032) electrode and an Ag/AgCl/KCl (3.0 M) (BAS Model MF-2078) electrode were employed as counter and reference electrodes, respectively. Gold substrates were used as the working electrodes. Prior to use, gold electrodes were cleaned according to the procedure described previously[36]. The electrolyte solutions were deaerated with high-purity nitrogen for 5 min before electrochemical experiments and kept in a nitrogen atmosphere during measurements.

The carbon films on gold substrates were produced by electrochemical reduction of polyhalogenated organic compounds. The electrolyte solutions were prepared by dissolving HCB, HCCP and their binary mixtures in acetonitrile solution containing 0.1 M $TBABF_4$. The molar concentrations of the HCB and HCCP solutions were 2 mM. The HCB/HCCP binary mixtures were prepared at 2/2, 2/1.2 and 2/0.6 molar ratios. The electrodes were then immersed in oxygen-free electrolyte solutions containing organic halides, and the carbon films were electrodeposited onto gold electrode surfaces either by potential-controlled electrolysis or by potential cycling between suitable cathodic potential limits. Then, in order to determine the thermal stability of the deposited films, the electrodes

This journal is © The Royal Society of Chemistry 20xx

modified by polymeric films were annealed at 400 ^{0}C for 30 min under an argon atmosphere. The as-deposited carbon films prepared with HCB, HCCP and HCB/HCCP binary mixtures were designated as PHCB, PHCCP and PHCB/PHCCP, respectively. After annealing, the films were designated as THCB, THCCP and THCB/THCCP.

Characterization

Scanning electron microscopy (SEM) images were obtained on a FEI Inspect S50 SEM. Raman measurements were collected on an inVia Reflex MicroRaman spectrometer (Renishaw), operating with a 532 nm Nd-YAG laser as the excitation source. X-ray photoelectron spectroscopy (XPS) studies were carried out with a SPECS (Berlin, Germany) spectrometer. Spectra were collected under ultrahigh vacuum conditions (1×10^{-9} Torr) using a constant analyzer energy mode (20 eV) with a monochromatic Al Kα (hν = 1486.6 eV) X-ray source. The binding energies were calibrated based on the C1s signal at 284.6 eV. BET surface area analysis was carried out with a Micromeritics 3Flex Surface Characterization Analyzer using nitrogen adsorption at 77 K. Mass spectrometry was performed using the Agilent 6530 Accurate Mass Q-TOF LC/MS system, operating in both positive and negative ion modes.

Electrochemical measurements

A three-electrode and a two-electrode setup were used to evaluate the capacitive properties of the synthesized carbon materials, respectively. In the three-electrode system, gold electrodes modified with carbon films were used in conjunction with a platinum wire counter electrode and an Ag/AgCl/KCl (3.0 M) reference electrode. In this system, 1 M Na_2SO_4 aqueous solution was used as the electrolyte. For the fabrication of the two-electrode symmetrical supercapacitor devices, firstly, the polymer films on gold electrodes were prepared by potential-controlled electrolysis in the solutions containing the HCB/HCCP binary mixtures. Next, these films were annealed at 400 ^{0}C, and then the annealed carbon films were completely stripped from the gold substrates. They were dispersed in ethanol and sonicated for 2 h. Afterthat, the suspension solutions were dropped onto the ITO electrode surfaces, and the solvent was allowed to completely evaporate in an oven at 60 ^{0}C for 30 min. The average weight of the active electrode materials on each electrode is about 4 mg. Then, the sandwich structures were performed by placing a laboratory filter paper as separator between two electrodes. 1 M Na_2SO_4 was used as the electrolyte. To avoid leakage of the electrolyte, the devices were wrapped with Teflon tape.

The cyclic voltammetry (CV), galvanostatic charge-discharge (GCD) and electrochemical impedance spectroscopy (EIS) experiments were performed on a Gamry Reference 600 electrochemical workstation. EIS was measured with a frequency range from 0.1 MHz to 10 Hz by applying an AC signal of 5 mV amplitude.

Conclusions

In conclusion, we have synthesized new carbon-based nanostructures by electrochemical reduction of polychlorinated hexagonal HCB and pentagonal HCCP organic molecules. Electrochemical reduction experiments were conducted in acetonitrile solutions containing HCB, HCCP and their mixtures at various molar ratios. The morphological, structural and capacitive properties of the resulting carbon coatings were evaluated by SEM, XPS, Raman, CV, GCD and EIS techniques. The results showed that using a simple electrochemical reduction method, different shapes of carbon nanostructures such as nanomushrooms, nanoflowers and nanolayers could be prepared by changing the type of the precursors and the molar ratio of the precursors. Moreover, it was found that the specific capacitances of these materials were comparable to the performances of many carbon-based materials reported in the literature.

Conflicts of interest

There are no conflicts to declare.

Acknowledgements

This research was financially supported by Atatürk University. We thank East Anatolia High Technology Application and Research Center for XPS measurements.

References

1 R. Jishi, M. Dresselhaus, G. Dresselhaus, *Phys. Rev. B*, 1993, **48**, 11385.
2 T. W. Ebbesen, H. J. Lezec, H. Hiura, J. W. Bennett, H. F. Ghaemi, T. Thio, *Nature*, 1996, **382**, 54.
3 Z. Yao, C. Kane, C. Dekker, *Phys. Rev. Lett.*, 2000, **84**, 2941.
4 A. H. Castro Neto, F. Guinea, N. Peres, K. Novoselov, A. Geim, *Rev. Mod. Phys.*, 2009, **81**, 109.
5 H. Kataura, Y. Maniwa, M. Abe, A. Fujiwara, T. Kodama, K. Kikuchi, H. Imahori, Y. Misaki, S. Suzuki, Y. Achiba, *Appl. Phys. A*, 2002, **74**, 349.
6 S. M. Bachilo, M. S. Strano, C. Kittrell, R. H. Hauge, R. E. Smalley, R. B. Weisman, *Science*, 2002, **298**, 2361.
7 C. Lee, X. Wei, J. W. Kysar, J. Hone, *Science*, 2008, **321**, 385.
8 C. Yan, J. Wang, W. Kang, M. Cui, X. Wang, C. Y. Foo, K. J. Chee, P. S. Lee, *Adv. Mater.*, 2014, **26**, 2022.
9 D. J. Lipomi, M. Vosgueritchian, B. C. K. Tee, S. L. Hellstrom, J. A. Lee, C. H. Fox, Z. Bao, *Nat. Nanotechnol.*, 2011, **6**, 788.
10 P. G. Collins, K. Bradley, M. Ishigami, A. Zettl, *Science*, 2000, **287**, 1801.
11 J. Kong, N. R. Franklin, C. Zhou, S. Peng, J. J. Cho, H. Dai, *Science*, 2000, **287,** 622.
12 W. Li, C. Liang, W. Zhou, J. Qiu, Z. Zhou, G. Sun, Q. Xin, *J. Phys. Chem. B*, 2003, **107**, 6292.
13 B. Seger, P. V. Kamat, *J. Phys. Chem. C*, 2009, **113**, 7990.
14 L. Qie, W. M. Chen, Z. H. Wang, Q. G. Shao, X. Li, L. X. Yuan, X. L. Hu, W. X. Zhang, Y. H. Huang, *Adv. Mater.*, 2012, **24**, 2047.
15 M. D. Stoller, S. Park, Y. Zhu, J. An, R. S. Ruoff, *Nano Lett.*, 2008, **8**, 3498.

16 J. Zhu, M. Chen, H. Wei, N. Yerra, N. Haldolaarachchige, Z. Luo, D. P. Young, T. C. Ho, S. Wei, Z. Guo, *Nano Energy*, 2014, **6**, 180.
17 X. Wang, Y. Ouyang, X. Li, H. Wang, J. Guo, H. Dai, *Phys. Rev. Lett.*, 2008, **100**, 206803/1-4.
18 F. Xia, D. B. Farmer, Y. Lin, P. Avouris, *Nano Lett.*, 2010, **10**, 715.
19 M. Bockrath, D. H. Cobden, P. L. Mc Euen, *Science*, 2000, **290**, 1552.
20 C. X. Guo, H. B. Yang, Z. M. Sheng, Z. S. Lu, Q. L. Song, C. M. Li, *Angew. Chem. Int. Ed.*, 2010, **49**, 3014.
21 J. Wei, Y. Jia, Q. Shu, Z. Gu, K. Wang, D. Zhuang, G. Zhang, Z. Wang, J. Luo, A. Cao, D. Wu, *Nano Lett.*, 2007, **7**, 2317.
22 R. B. Ross, C. M. Cardona, D. M. Guldi, S. G. Sankaranarayanan, M. O. Reese, N. Kopidakis, J. Peet, B. Walker, G. C. Bazan, E. V. Keuren, B. C. Holloway, M. Drees, *Nat. Mater.*, 2009, **8**, 208.
23 H. W. Kroto, J. R. Heath, S. C. Obrien, R. F. Curl, R. E. Smalley, *Nature*, 1985, **318**, 162.
24 S. Iijima, *Nature*, 1991, **354**, 56.
25 H. W. Kroto, *Nature*, 1992, **359**, 670.
26 O. Mykhailiv, H. Zubyk, M. E. Plonska-Brzezinska, *Inorg. Chim. Acta*¸ 2017, **468**, 49.
27 J. R. Hester, O. A. Louchev, *Appl. Phys. Lett.*, 2002, **80**, 2580.
28 M. Endo, H.W. Kroto, *J. Phys. Chem.*, 1992, **96**, 6941.
29 S. Bandow, A. M. Rao, G. U. Sumanasekera, P. C. Eklund, F. Kokai, K. Takahashi, M. Yudasaka, S. Iijima, *Appl. Phys. A-Mater. Sci. Process.*, 2000, **71**, 561.
30 A. G. Nasibulin, P. V. Pikhitsa, H. Jiang, D. P. Brown, A. V. Krasheninnikov, A. S. Anisimov, P. Queipo, A. Moisala, D. Gonzalez, G. Lientschnig, A. Hassanien, S. D. Shandakov, G. Lolli, D. E. Resasco, M. Choi, D. Tománek, E. I. Kauppinen, *Nature Nanotech.*, 2007, **2**, 156.
31 W. Wang, K. Q. Yang, J. Gaillard, P. R. Bandaru, A. M. Rao, *Adv. Mater.*, 2008, **20**, 179.
32 Y. Qin, Z. K. Zhang, Z. L. Cui, *Carbon,* 2003, **41**, 3063.
33 X. Armand, N. Herlin, I. Voicu, M. Cauchetier, *J. Phys. Chem. Solids*¸ 1997, **58**, 1853.
34 Z. K. Kang, E. Wang, B. Mao, Z. Su, L. Gao, S. Lian, L. Xu, *J. Am. Chem. Soc.*, 2005, **127**, 6534.
35 G. Che, B. B. Lakshmi, C. R. Martin, E. R. Fisher, R. S. Ruoff, *Chem. Mater.*, 1998, **10**, 260.
36 Z. Kudaş, E. Gür, D. Ekinci, *Langmuir*, 2018, **34**, 7958.
37 E. Papirer, R. Lacroix, J. B. Donnet, G. Nanse, P. Fioux, *Carbon*, 1995, **33**, 63.
38 A. Sadezky, H. Muckenhuber, H. Grothe, R. Niessner, U. Pöschl, *Carbon*, 2005, **43**, 1731.
39 R. Al-Jishi, G. Dresselhaus, *Phys. Rev. B*, 1982, **26**, 4514.
40 A. Cuesta, P. Dhamelincourt, J. Laureyns, A. Martinez-Alonso, J. M. D. Tascon, *Carbon*, 1994, **32**, 1523.
41 T. Jawhari, A. Roid, J. Casado, *Carbon*, 1995, **33**, 1561.
42 B. Dippel, H. Jander, J. Heintzenberg, *Phys. Chem. Chem. Phys.*, 1999, **1**, 4707.
43 S. W. Lee, N. Yabuuchi, B. M. Gallant, S. Chen, B. S. Kim, P. T. Hammond, Y. Shao-Horn, *Nature Nanotech.*, 2010, **5**, 531.
44 L. G. Austin, E. G. Gagnon, *J. Electrochem. Soc.*, 1973, **120**, 251.
45 J. Xu, Z. Tan, W. Zeng, G. Chen, S. Wu, Y. Zhao, K. Ni, Z. Tao, M. Ikram, H. Ji, Y. Zhu, *Adv. Mater.*, 2016, **28**, 5222.
46 E. Feng, H. Peng, Z. Zhang, J. Li, Z. Lei, *New J. Chem.*, 2017, **41**, 9024.
47 Y. Bu, T. Sun, Y. Cai, L. Du, O. Zhuo, L. Yang, Q. Wu, X. Wang, Z. Hu, *Adv. Mater.*, 2017, **29**, 1700470/1-7.
48 J. G. Wang, H. Liu, X. Zhang, M. Shao, B. Wei, *J. Mater. Chem. A*, 2018, **6**, 17653.
49 V. V. V. Obreja, *Physica E*, 2008, **40**, 2596.
50 S. Haladkar, P. Alegaonkar, *Appl. Surf. Sci.*, 2018, **449**, 500.
51 M. D. Stoller, R. S. Ruoff, *Energy Environ. Sci.*, 2010, **3**, 1294.
52 J. Fang, X. Miao, X. Zhang, Y. Liu, S. Chen, Y. Chen, W. Wang, Y. Zhang, *J. Power Sources*¸ 2019, **418**, 24.
53 S. Wang, B. Pei, X. Zhao, R.A.W. Dryfe, *Nano Energy*, 2013, **2**, 530.
54 G. Suna, B. Lia, J. Rana, X. Shena, H. Tonga, *Electrochim. Acta*, 2015, **171**, 13.
55 F. Ma, D. Ma, G. Wu, W. Geng, J. Shao, S. Song, J. Wana, J. Qiu, *Chem. Commun.*, 2016, **52**, 6673.
56 Y. Cheng, L. Huang, X. Xiao, B.Yao, L.Yuan, T. Li, Z. Hu, B. Wang, J. Wan, J. Zhou, *Nano Energy*¸ 2015, **15**, 66.
57 Q. Wang, B. Qin, X. Zhang, X. Xie, L. Jin, Q. Cao, *J. Mater. Chem. A*, 2018, **6**, 19653.
58 Y. Cai, Y. Luo, Y. Xiao, X. Zhao, Y. Liang, H. Hu, H. Dong, L. Sun, Y. Liu, M. Zheng, *ACS Appl. Mater. Interfaces*, 2016, **8**, 33060.

This journal is © The Royal Society of Chemistry 20xx

Please do not adjust margins

Electronic Supplementary Information for:

Production of novel carbon nanostructures by electrochemical reduction of polychlorinated organic rings under mild conditions for supercapacitors

Züleyha Kudaş[a], Emir Çepni[b], Emre Gür[c] and Duygu Ekinci*[a]

[a]Department of Chemistry, Faculty of Sciences, Atatürk University, 25240 Erzurum. Turkey.

[b] Department of Nanoscience and Nanoengineering, Nanomaterials Sciences, Atatürk University, 25240 Erzurum, Turkey.

[c]Department of Physics, Faculty of Sciences, Atatürk University, 25240 Erzurum. Turkey.

Corresponding author e-mail address: dekin@atauni.edu.tr

Table of Contents

ESI1. Electrochemical Reduction of Hexachlorocyclopentadiene (HCCP).....S2
ESI2. Electrochemical Reduction of HCB/HCCP Mixtures S8
ESI3. SEM Images of PHCB/PHCCP Films.....S9
ESI4. XPS Analysis of Carbon Films.....S13
ESI5. Raman Analysis of Carbon Films S16
ESI6. Capacitive Performances of Carbon Films.....S17
ESI7. Surface Area and Porosity Characteristics of Carbon Films S23
ESI8. References S24

ESI1. Electrochemical Reduction of Hexachlorocyclopentadiene (HCCP)

The electrochemical reduction behaviour of HCCP was investigated by cyclic voltammetry. Fig. S1 shows a typical cyclic voltammogram obtained in acetonitrile solution containing 2 mM HCCP and 0.1 M $TBABF_4$ at a gold electrode. As seen, the voltammogram exhibits a well-defined irreversible cathodic peak at -0.73 V followed by a series of small reduction peaks at -1.15, -1.47 and -1.86 V vs. Ag/AgCl/KCl (3.0 M).

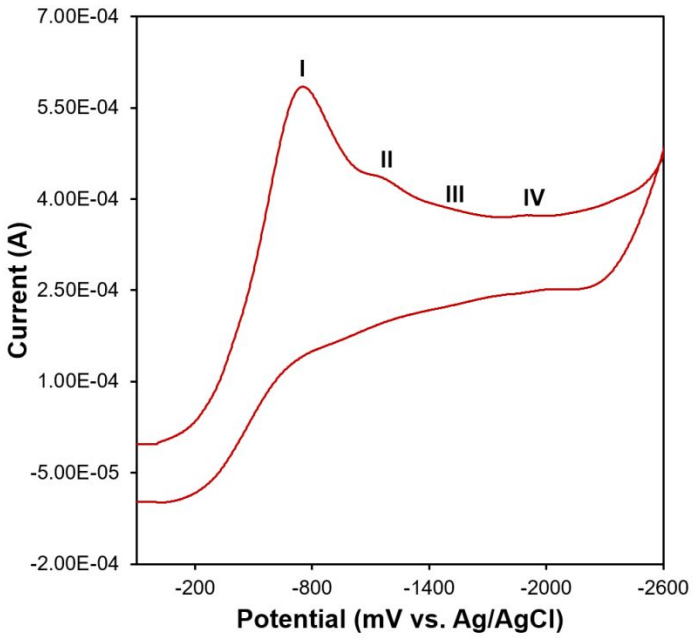


Fig. S1 Cyclic voltammogram of HCCP in acetonitrile containing 0.1 M $TBABF_4$. The scan rate is 0.1 V s^{-1}.

The electroreductive dehalogenation process of HCCP in aqueous buffer solution has been previously reported by Bedioui *et al.*[1] They noted that electrocatalytic reduction of HCCP at HOPG electrode modified with DDAB/Hemin surfactant film showed an irreversible cathodic wave with a peak potential of -1.10 V vs. SCE. This potential is significantly more negative than that observed in our experiments (-0.73 V vs. Ag/AgCl/KCl (3.0 M)). The significant positive shift in the reduction potential can associated with the catalytic effect of the gold electrode.[2]

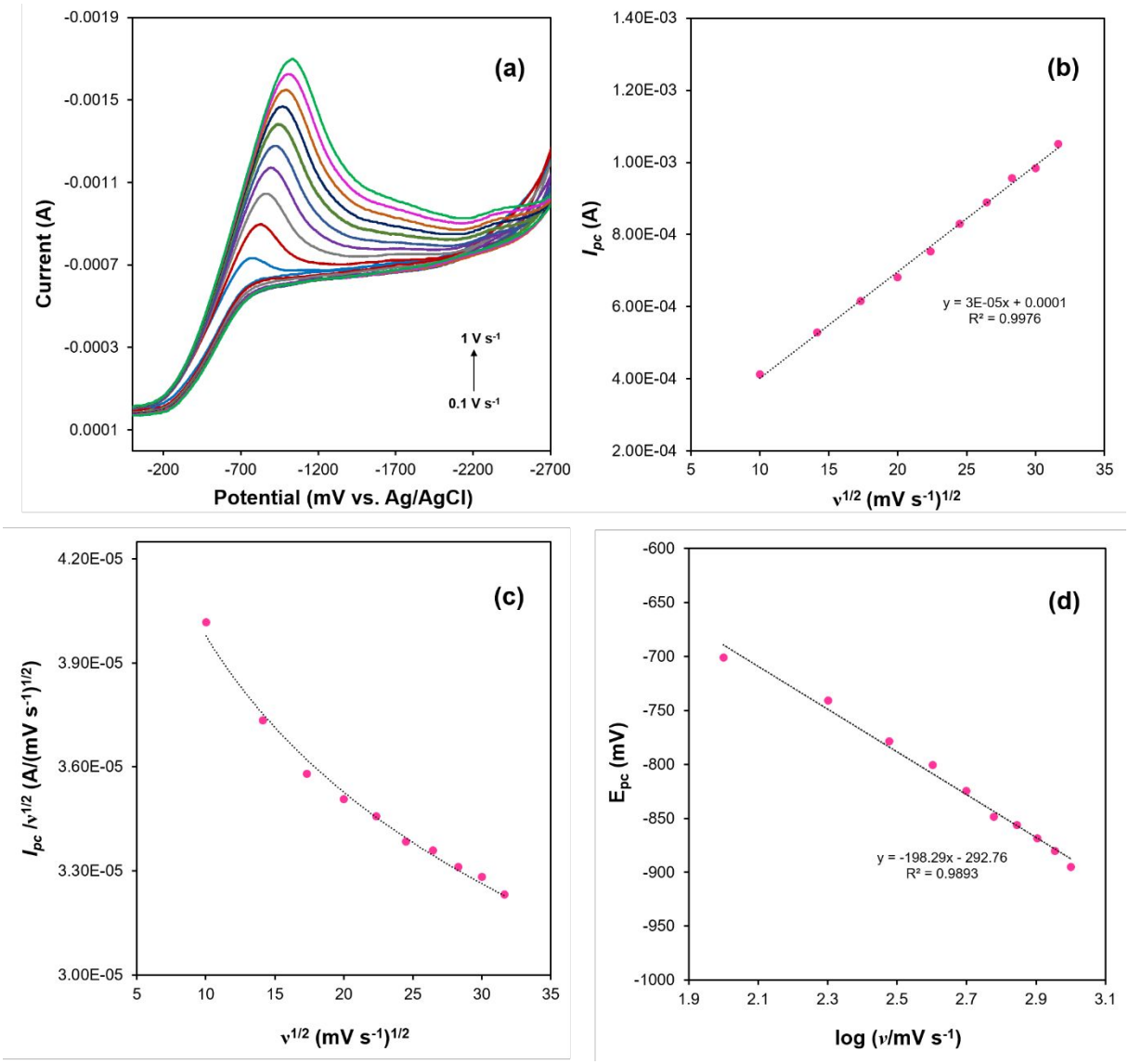


Fig. S2 (a) Cyclic voltammograms recorded at different scan rates in acetonitrile solution containing 2 mM HCCP and 0.1 M $TBABF_4$. (b) Variation of cathodic peak current with square root of scan rate for the first peak. (c) Variation of the current function ($I_{pc}/\nu^{1/2}$) with the square root of the scan rate ($\nu^{1/2}$) for the first peak. (d) Variation of the cathodic peak potential with the logarithm of scan rate for the first peak.

To further understand the electrochemical reduction behaviour of HCCP on gold electrodes, a series of the cyclic voltammograms were recorded at different scan rates (0.1-1.0 V s^{-1}) in acetonitrile solution containing 2 mM HCCP and 0.1 M $TBABF_4$ (Fig. S2a). As seen in Fig. S2a, the cathodic

peak currents increase as the scan rate is increased. In addition, the cathodic peak potentials shift to more negative potentials with increasing scan rate. For the first peak, the plot of the cathodic peak current (I_{pc}) versus the square root of the scan rate ($\nu^{1/2}$) is linear (Fig. S2b), and also the current function ($I_{pc}/\nu^{1/2}$) decrease with increasing $\nu^{1/2}$ (Fig. S2c). These observations indicate that the nature of redox process is diffusion controlled and electron transfer is followed by a chemical reaction.

In order to find the rate-determining step during the reduction process of HCCP, the electron transfer coefficient (α) was calculated from cyclic voltammograms using the variation of cathodic peak potential (E_{pc}) with logarithm of scan rate (log ν) according to Eq. 1,

$$\mathbf{E_{pc} = -\frac{1.151RT}{\alpha F}\log\nu} \quad (1)$$

where *R* is the gas constant (8.314 J K^{-1} mol^{-1}); T is the room temperature (298 K) and F is the Faraday constant (96500 C mol^{-1}). Fig. S2d shows the variation of E_{pc} as a function of log ν. From the slope of the graph, the α value was calculated to be 0.15 for HCCP, suggesting that electron transfer process is the rate-determining step, and thus that the reduction occurs through a concerted mechanism.[2-5]

To determine the number of electrons transferred (n) during the electrochemical reduction of HCCP, chronocoulometry experiments were performed. Experiments were conducted by applying potential steps from 0.0 V to -0.7 V and to -2.9 V vs. Ag/AgCl/KCl (3.0 M) in the time domain from 0.5 to 16 s. Fig. S3a shows representative chronocoulometry curves recorded by stepping the applied potential from 0.0 V to -2.9 V. As shown, the total charge (Q) gradually increases with time (t). Also, the Q values for both applied step potentials are linearly proportional to the value of $t^{1/2}$ (Fig. S3b). The n values were calculated from Q vs. $t^{1/2}$ plots using Anson equation (Eq.2),[6]

$$\mathbf{Q = \frac{2nFAC_0D^{1/2}}{\pi^{1/2}}t^{1/2}} \quad (2)$$

where Q is the charge (C); n is the number of electrons transferred; F is Faraday's constant (96500 C mol^{-1}); A is the area of the working electrode; C_0 is the bulk concentration of HCCP (2×10^{-6} mol cm^{-3})

and D is diffusion coefficient (taken to be 1.0×10^{-5} cm^2 s^{-1}). Thus, the n values were found to be 4.5 and 12.4 for the step potentials of -0.7 V and -2.9 V vs. Ag/AgCl/KCl (3.0 M), respectively.

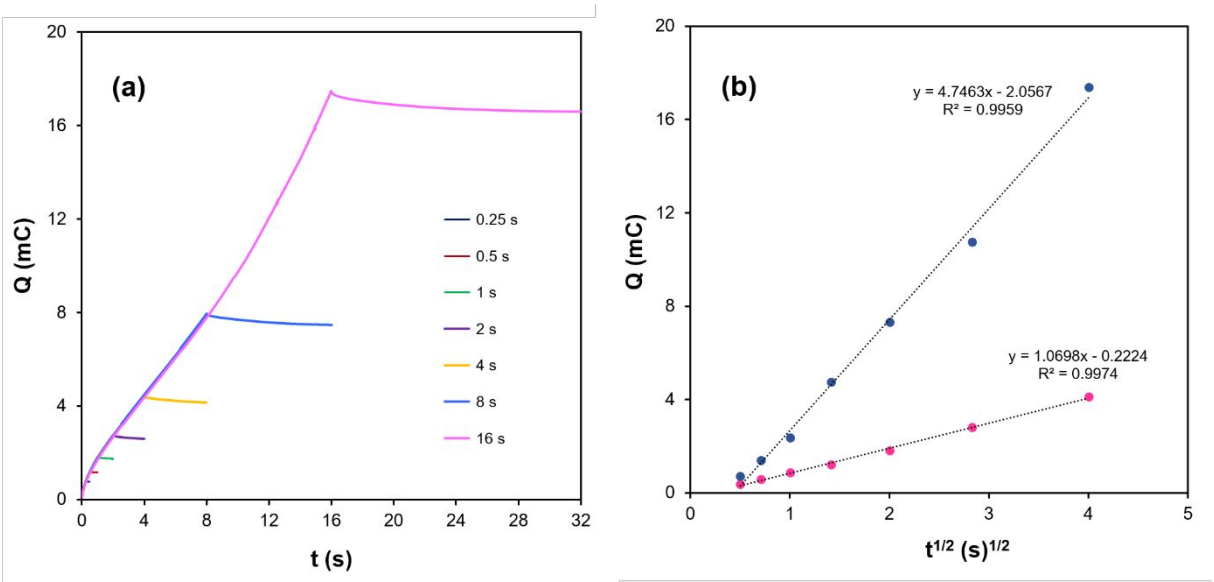


Fig. S3 (a) Chronocoulograms recorded in acetonitrile containing 2 mM HCCP and 0.1 M $TBABF_4$ at different time domains. The potential was stepped from 0.0 V to -2.9 V. (b) The plots of the total charge (Q) versus $t^{1/2}$ for HCCP at the same conditions. The potentials were stepped from 0.0 V to -0.7 V (•) and to -2.9 V (•).

The catalytic reduction of HCCP has been previously studied in the presence of metal and/or metal salts such as zinc, copper, copper chloride and tin chloride as reducing agents.[7-10] The HCCP is reduced in a stepwise manner to 1,2,3,4,5-pentachlorocyclopentadiene (PCCP) and 1,2,3,4-tetrachlorocyclopentadiene (TCCP) with zinc in HCl solution.[7,8] Since these molecules (PCCP and TCCP) can act both as dienes and dienophiles in the Diels-Alder reactions, they slowly undergoes cycloaddition with themselves to give [2.2.1]bicycloheptene derivatives under relatively mild conditions. Besides, HCCP is subjected to homogeneous bimolecular reductive coupling reaction by copper and copper chloride to yield bis-(pentachlorocyclopentaadienyl) (bis-PCCP).[9,10]

In this regard, to elucidate the nature of products obtained from the electrochemical reduction of HCCP, potential-controlled electrolysis experiments were conducted at -0.7 V and -2.9 V vs.

Ag/AgCl/KCl (3.0 M) in acetonitrile solution containing 2 mM HCCP and 0.1 M $TBABF_4$. After electrolysis for 2 h, electrolyte solutions were analysed by Q-TOF LC/MS (Fig. S4). As shown, the mass spectra display two prominent peaks at m/z 242.28 and 571.59 as well as several lower intensity peaks at higher masses. The peak at m/z 242.28 is the molecular ion peak caused by the cation of the $TBABF_4$.[11] The prominent peak at m/z 571.59 and other small peaks in the spectra can be attributed to the [2.2.1]bicycloheptene structures produced by Diels-Alder cycloaddition reactions of cyclopentadiene derivatives generated during electrolysis.[12-14]

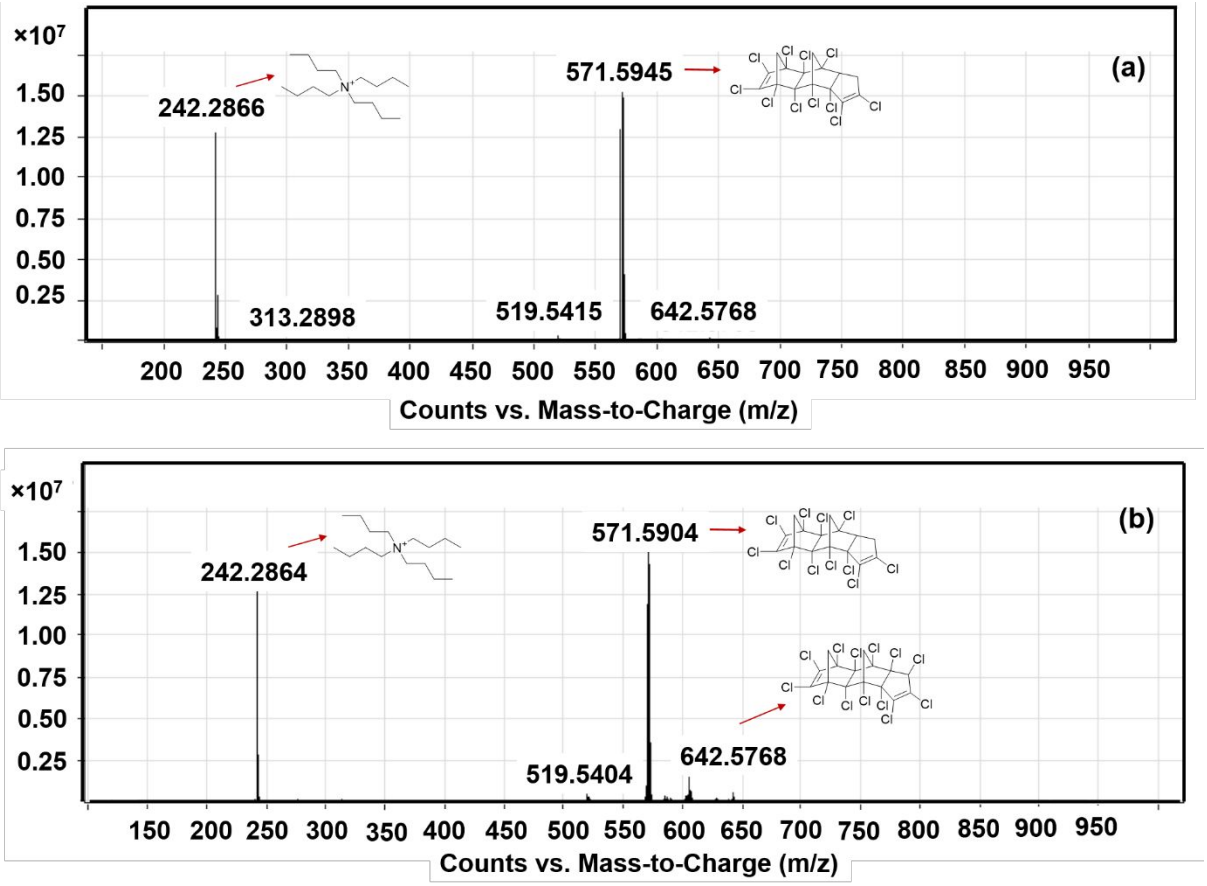
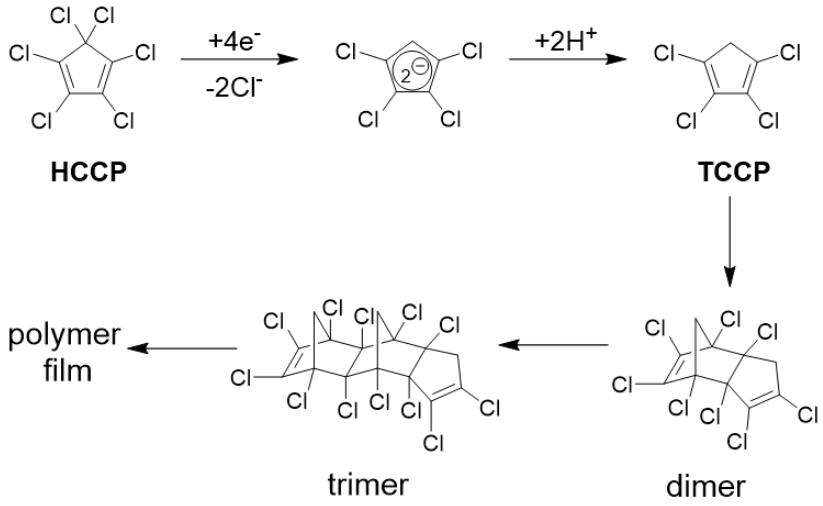


Fig. S4 Q-TOF LC/MS analysis of the electrolysis solutions of HCCP and its possible reaction products. Potential-controlled electrolysis experiments were performed at (a) -0.7 V and (b) -2.9 V vs. Ag/AgCl/KCl (3.0 M) in acetonitrile solution containing 2 mM HCCP and 0.1 M $TBABF_4$.

On the basis of the experimental results, it appears that the first step of the electrochemical reduction process is addition of four electrons to HCCP followed by a concerted mechanism where the electron transfer and the C-Cl bond dissociation are simultaneous (Scheme S1). The concerted decomposition leads to the formation of the corresponding dianion and chloride ions. The produced dianion is rapidly protonated by residual water or some other proton sources to form the final product TCCP. The diene TCCP is an excellent cyclic diene for Diels-Alder reaction with dienophiles, and thus it reacts with itself (or with HCCP or its different reduction states such as trichlorocyclopentadiene, dichlorocyclopentadiene and cyclopentadiene) to produce norbornene derivatives. By repeating this process, the growth of the polymer film occurs on the electrode surface.



Scheme S1. Proposed reaction scheme for the electrochemical reduction of HCCP.

ESI2. Electrochemical Reduction of HCB/HCCP Mixtures

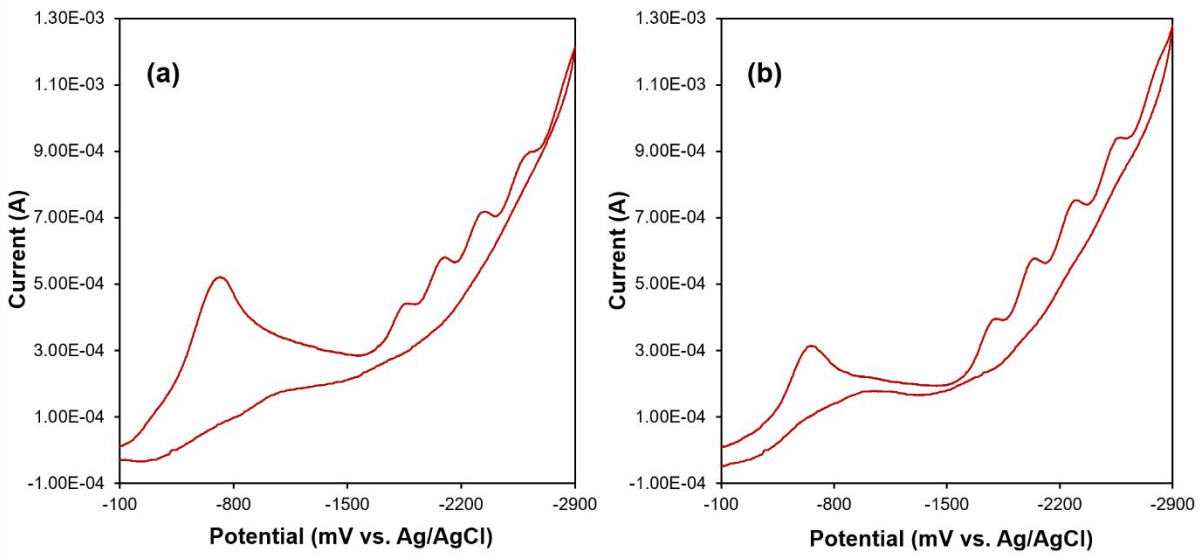


Fig. S5 Cyclic voltammetric responses for mixtures of HCB and HCCP at the molar ratios of (a) 2/1.2 and (b) 2/0.6 in acetonitrile containing 0.1 M $TBABF_4$ with scan rate of 0.1 V s^{-1} at gold electrodes.

EIS3. SEM Images of PHCB/PHCCP Films

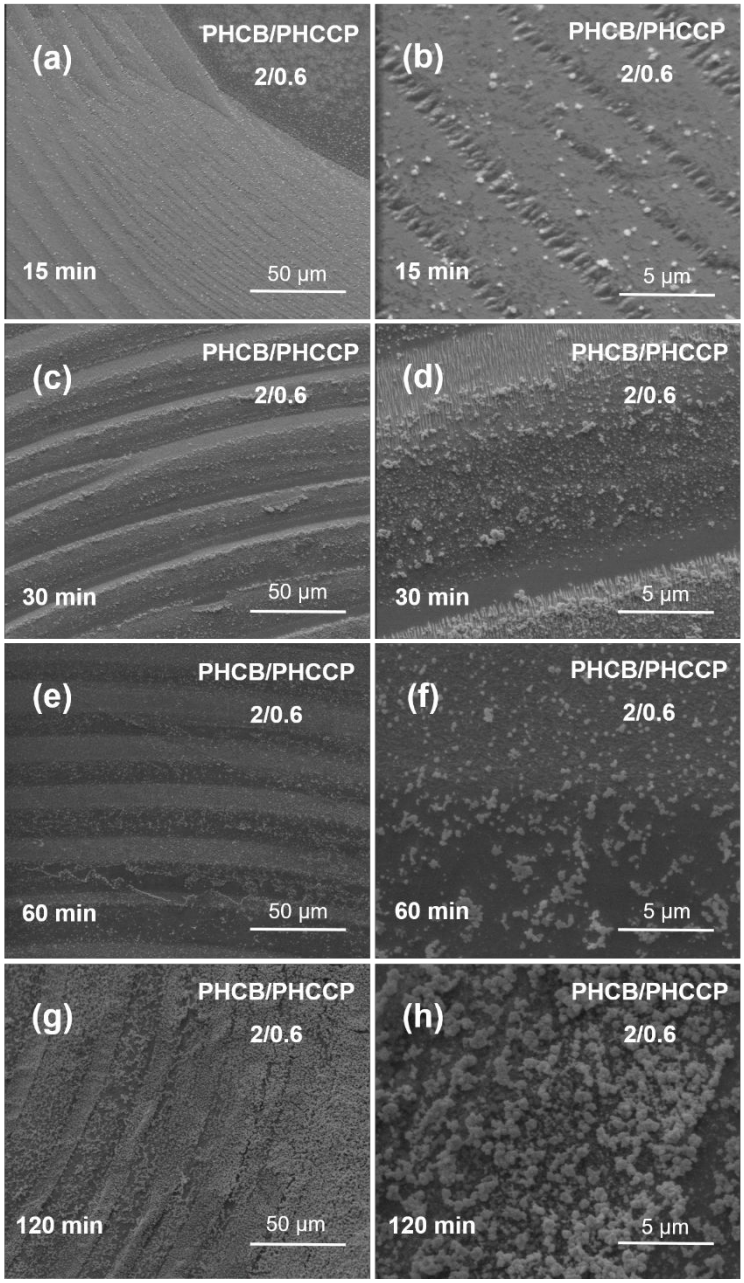


Fig. S6 SEM images of carbon films obtained by potential-controlled electrolysis in 0.1 M $TBABF_4$/acetonitrile solution containing 2 mM HCB and 0.6 mM HCCP. For a 15 min deposition time, the small polymer particles concentrated at the step edges of the gold were observed. As the electrolysis time increases, a greater density of the larger particles was formed on the electrode surface. At the end of 120 min electrolysis, the surface was covered with irregular-shaped particles.

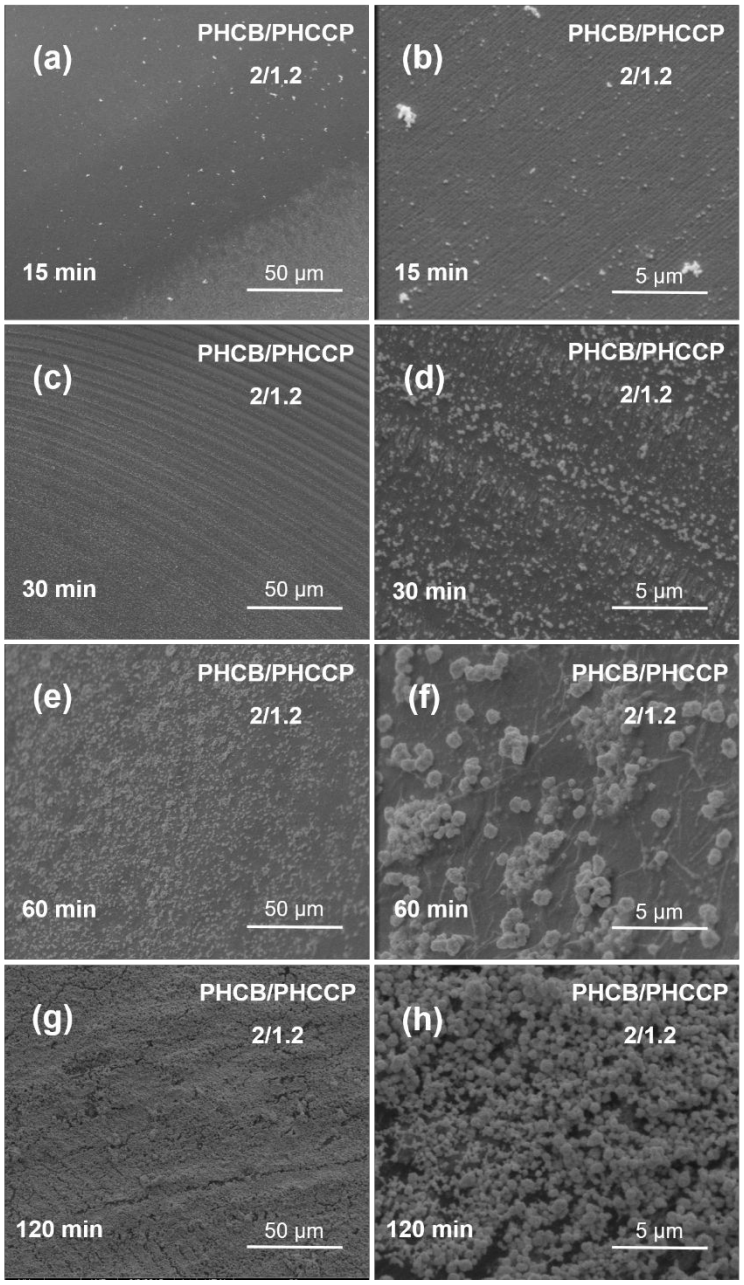


Fig. S7 SEM images of carbon films obtained by potential-controlled electrolysis in 0.1 M $TBABF_4$/acetonitrile solution containing 2 mM HCB and 1.2 mM HCCP. After 15 min of deposition, a smooth coating containing small particles was observed. With increasing electrolysis time, the particle size and density increased, and the smooth film on the electrode surface transformed to the crumpled form. At the end of 120 min electrolysis, the surface was covered with nanoflower-like carbon particles of various sizes.

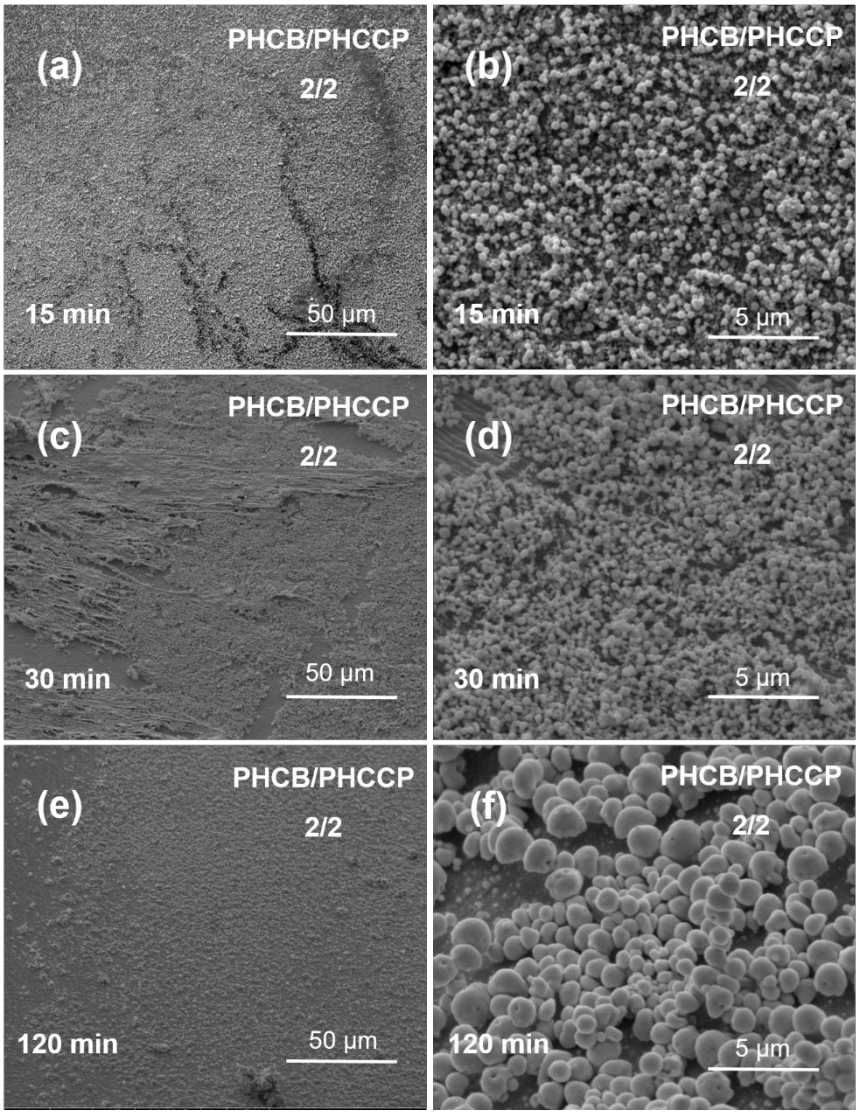


Fig. S8 SEM images of carbon films obtained by potential-controlled electrolysis in 0.1 M $TBABF_4$/acetonitrile solution containing 2 mM HCB and 2 mM HCCP. After the first 15 min of deposition, the gold surface was densely covered with spherical particles. After 30 min of deposition, the particles gathered together, and also the presence of a laminar layer similar to that observed in the PHCCP film was obtained on the electrode surface. At the end of 120 min electrolysis, the particles transformed to the nanomushroom-like structures.

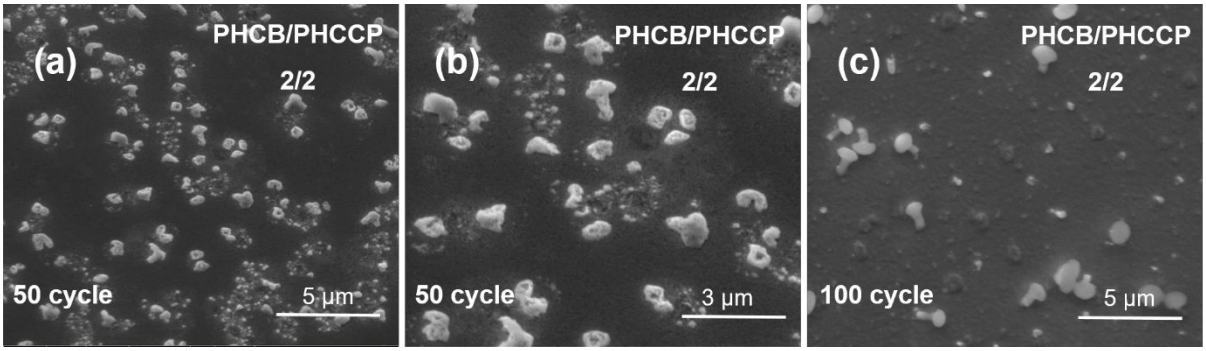


Fig. S9 SEM images of carbon films obtained by potential cycling between -0.1 and -2.9 V at a scan rate of 0.1 V s^{-1} in 0.1 M $TBABF_4$/acetonitrile solution containing 2 mM HCB and 2 mM HCCP.

ESI4. XPS Analysis of Carbon Films

Table S1. XPS analysis parameters obtained from the C1s spectra.

sample		Csp^2	Csp^3	C-Cl
PHCB	peak center (eV)	283.5	284.8	286.9
	fwhm	1.73	1.88	2.19
	atomic%	39.42	33.24	27.35
THCB	peak center (eV)	283.9	285.1	287.5
	fwhm	1.47	1.89	1.87
	atomic%	64.05	25.07	10.87
PHCCP	peak center (eV)	284.1	285.4	287.1
	fwhm	1.75	1.80	1.94
	atomic%	38.91	41.56	19.54
THCCP	peak center (eV)	284.0	285.3	287.2
	fwhm	1.53	1.76	1.91
	atomic%	54.64	32.92	12.43
PHCB/PHCCP (2/0.6)	peak center (eV)	283.8	285.5	286.6
	fwhm	2.06	1.54	1.68
	atomic%	54.76	27.07	18.18
THCB/THCCP (2/0.6)	peak center (eV)	283.9	285.0	286.6
	fwhm	1.44	1.62	1.44
	atomic%	57.68	32.39	9.92
PHCB/PHCCP (2/1.2)	peak center (eV)	283.7	285.1	286.8
	fwhm	1.82	1.82	1.82
	atomic%	54.13	31.13	14.74
THCB/THCCP (2/1.2)	peak center (eV)	284.2	285.5	287.3
	fwhm	1.44	1.80	1.66
	atomic%	57.09	31.13	11.77
PHCB/PHCCP (2/2)	peak center (eV)	283.4	285.0	286.6
	fwhm	1.88	1.78	1.65
	atomic%	60.93	27.92	11.15
THCB/THCCP (2/2)	peak center (eV)	283.9	285.4	287.6
	fwhm	1.52	1.82	1.90
	atomic%	70.59	20.50	8.90

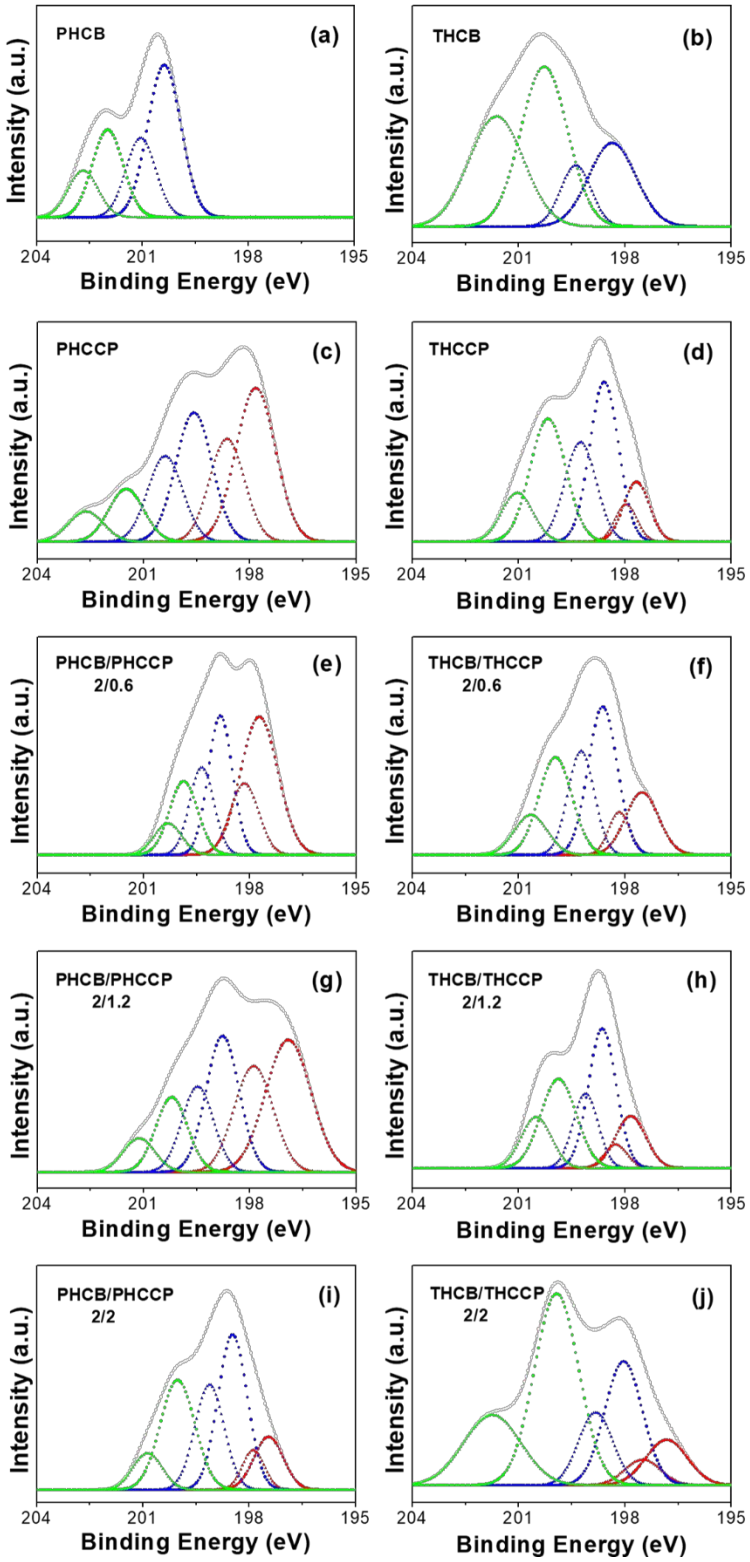


Fig. S10 Deconvoluted Cl2p XPS spectra of carbon films deposited by 120 min electrolysis before and after annealing at 400 ^{0}C.

Table S2. XPS analysis parameters obtained from the Cl2p spectra.

sample		$Cl2p_{3/2}$ ($C\text{-}Cl_2$)	$Cl2p_{1/2}$ ($C\text{-}Cl_2$)	$Cl2p_{3/2}$ ($Csp^3\text{–}Cl$)	$Cl2p_{1/2}$ ($Csp^3\text{–}Cl$)	$Cl2p_{3/2}$ ($Csp^2\text{-}Cl$)	$Cl2p_{1/2}$ ($Csp^2\text{-}Cl$)
PHCB	peak center (eV)	-	-	200.4	201.0	201.9	202.7
	fwhm	-	-	1.11	0.99	1.03	0.99
	atomic%	-		64.44		35.56	
THCB	peak center (eV)	-	-	198.4	199.4	200.3	201.6
	fwhm	-	-	1.55	1.02	1.55	1.81
	atomic%	-		30.05		69.95	
PHCCP	peak center (eV)	197.8	198.6	199.6	200.4	201.5	202.6
	fwhm	1.31	1.16	1.21	1.16	1.16	1.16
	atomic%	47.65		37.99		14.35	
THCCP	peak center (eV)	197.7	197.9	198.6	199.2	200.2	201.0
	fwhm	0.86	0.72	0.95	1.04	1.18	1.04
	atomic%	14.80		48.27		36.93	
PHCB/PHCCP (2/0.6)	peak center (eV)	197.7	198.1	198.8	199.4	199.9	200.3
	fwhm	1.24	0.95	0.81	0.81	0.94	0.90
	atomic%	45.92		35.22		18.86	
THCB/THCCP (2/0.6)	peak center (eV)	197.5	198.2	198.6	199.2	199.9	200.7
	fwhm	1.09	0.71	0.96	0.87	1.09	1.09
	atomic%	20.41		48.29		31.29	
PHCB/PHCCP (2/1.2)	peak center (eV)	196.9	197.9	198.8	199.5	200.2	201.1
	fwhm	1.51	1.29	1.10	1.06	1.06	1.06
	atomic%	48.64		34.75		16.61	
THCB/THCCP (2/1.2)	peak center (eV)	197.8	198.3	198.6	199.1	199.9	200.5
	fwhm	1.00	0.75	0.91	0.83	1.18	1.00
	atomic%	16.81		45.61		37.58	
PHCB/PHCCP (2/2)	peak center (eV)	197.4	197.9	198.5	199.1	200.0	200.9
	fwhm	0.97	0.73	0.97	0.97	1.14	0.97
	atomic%	16.27		51.15		32.58	
THCB/THCCP (2/2)	peak center (eV)	196.8	197.5	198.0	198.8	199.9	201.7
	fwhm	1.38	1.19	1.24	1.14	1.47	1.89
	atomic%	12.50		31.78		55.72	

ESI5. Raman Analysis of Carbon Films

Table S3. Raman peak positions (cm^{-1}) for the carbon films.

sample	peak I	peak II	peak III	peak IV	peak V	peak VI	peak VII
PHCB	1126.6	1234.1	1288.8	1339.3	1432.9	1568.8	1623.3
THCB	1140.9	1215.9	1275.4	1344.6	1410.5/ 1467.8	1563.1	1621.0
PHCCP	1135.0	1229.0	1296.8	1361.2	1449.3	1573.1	1625.5
THCCP	1118.5	1212.0	1292.6	1366.1	1459.1	1578.4	1619.6
THCB/THCCP (2/0.6)	1014.4	1107.4	1213.5	1343.9	1459.1	1562.2	1623.1
THCB/THCCP (2/1.2)	1057.0	1144.9	1237.8	1355.2	1465.9	1568.8	1625.3
THCB/THCCP (2/2)	1074.7	1155.2	1238.0	1348.6	1466.4	1574.3	1620.5

ESI6. Capacitive Performances of Carbon Films

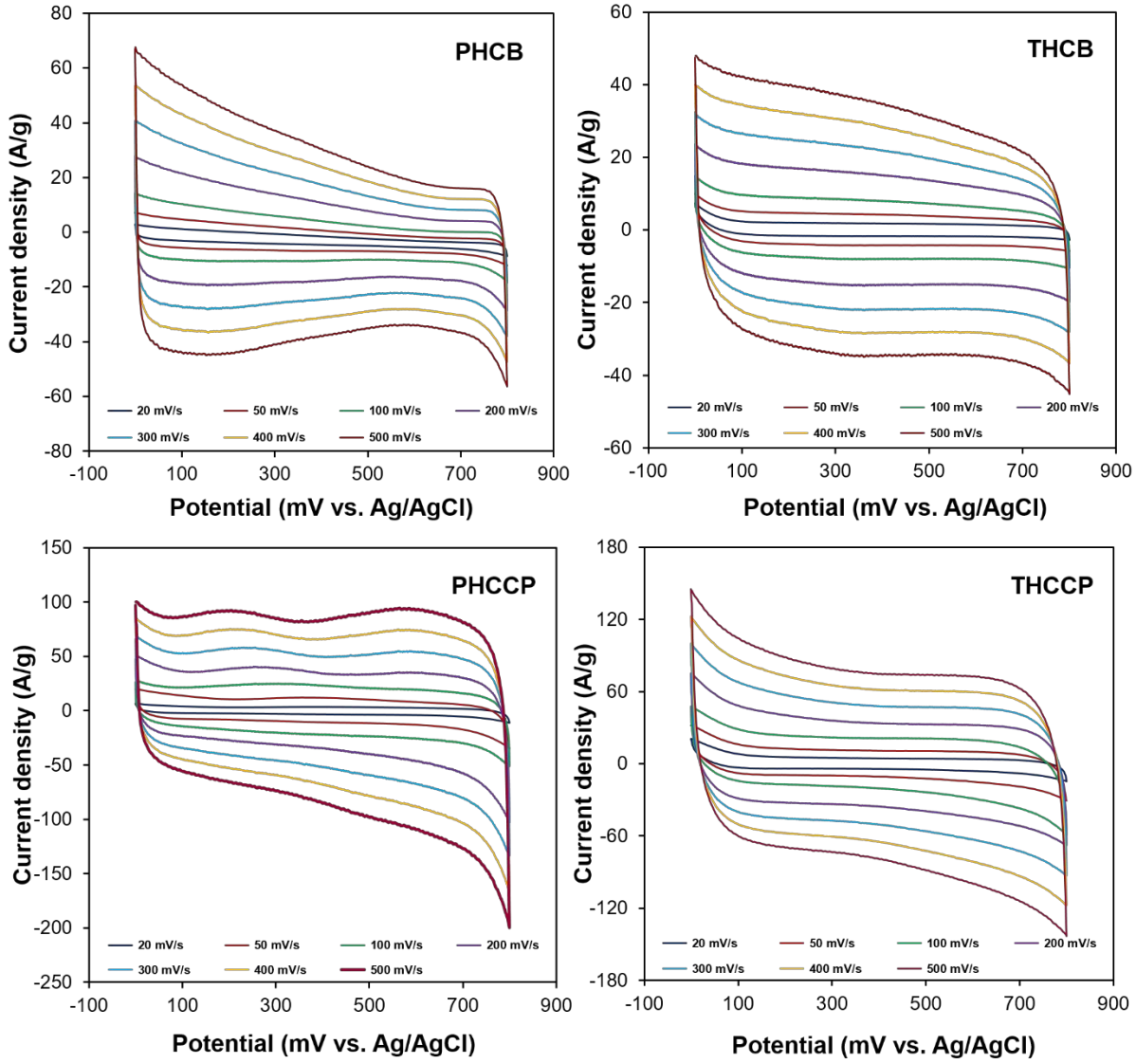


Fig. S11 CV curves recorded for PHCB/Au, THCB/Au, PHCCP/Au and THCCP/Au electrodes in 1 M Na_2SO_4 aqueous solution at different scan rates (20 to 500 mV s^{-1}).

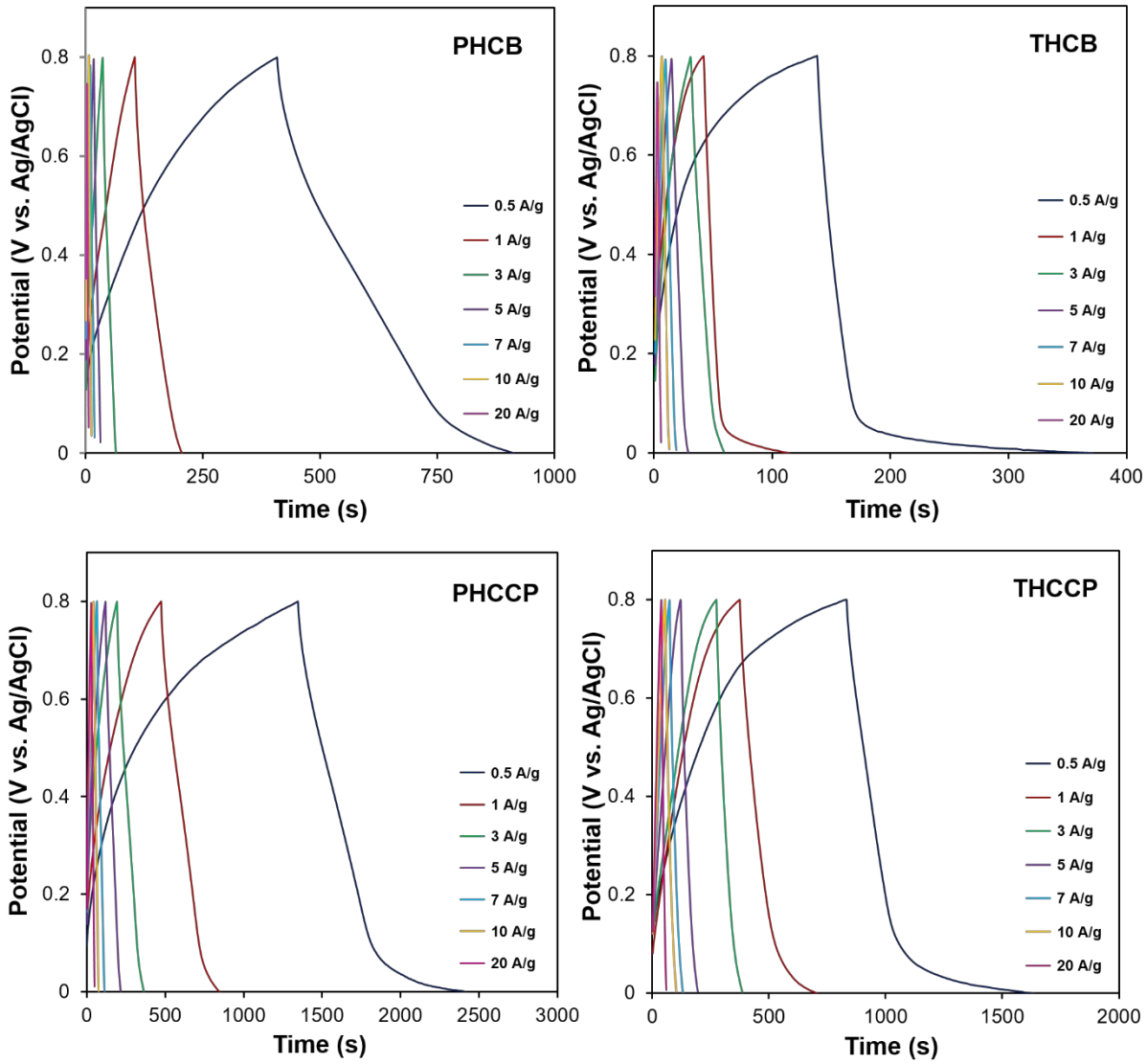


Fig. S12 GCD curves recorded for PHCB/Au, THCB/Au, PHCCP/Au and THCCP/Au electrodes in 1 M Na_2SO_4 aqueous solution at different current densities (0.5 A g^{-1} to 20 A g^{-1}).

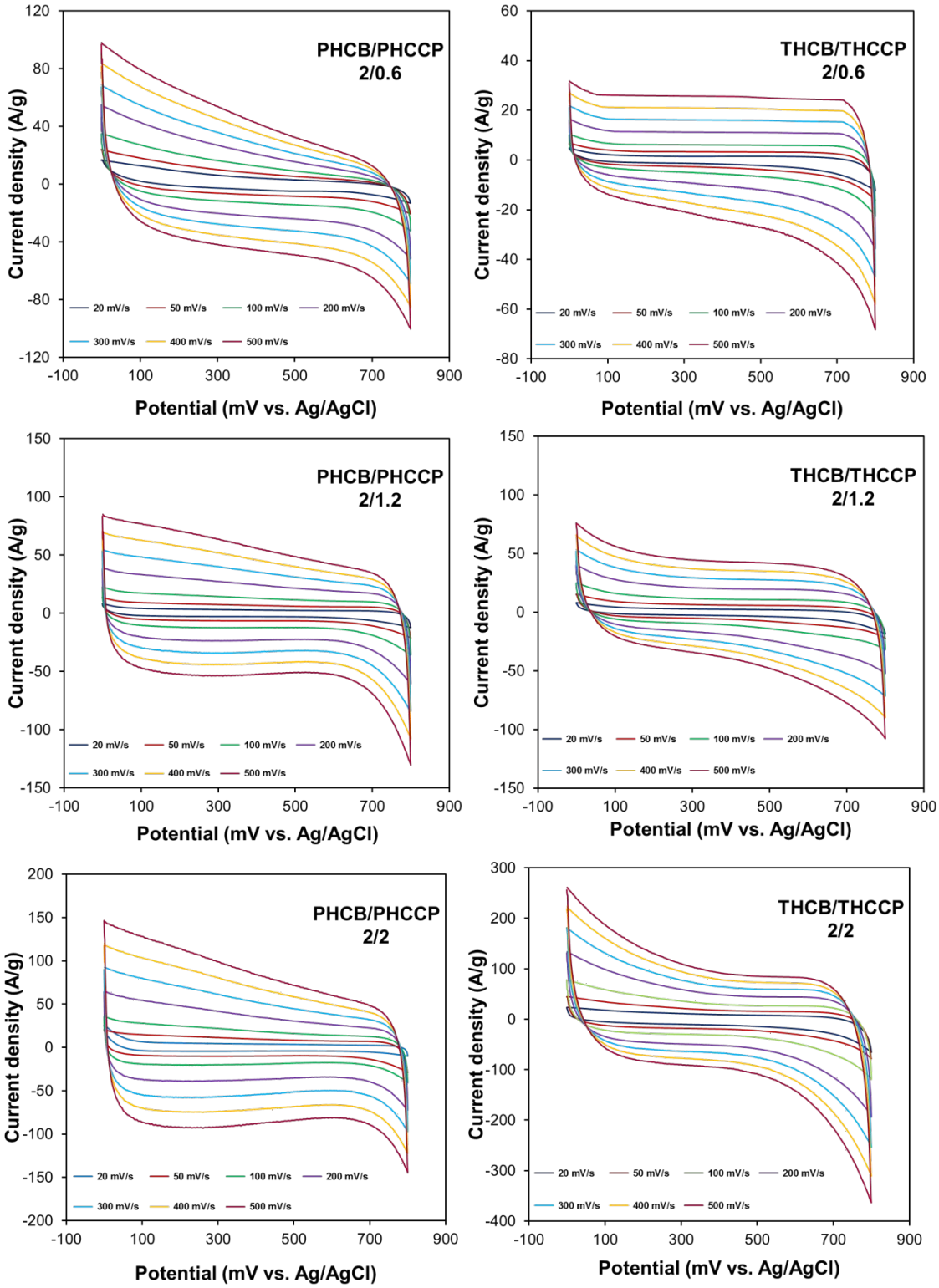


Fig. S13 CV curves recorded for the carbon films in 1 M Na_2SO_4 aqueous solution at different scan rates (20 to 500 mV s^{-1}).

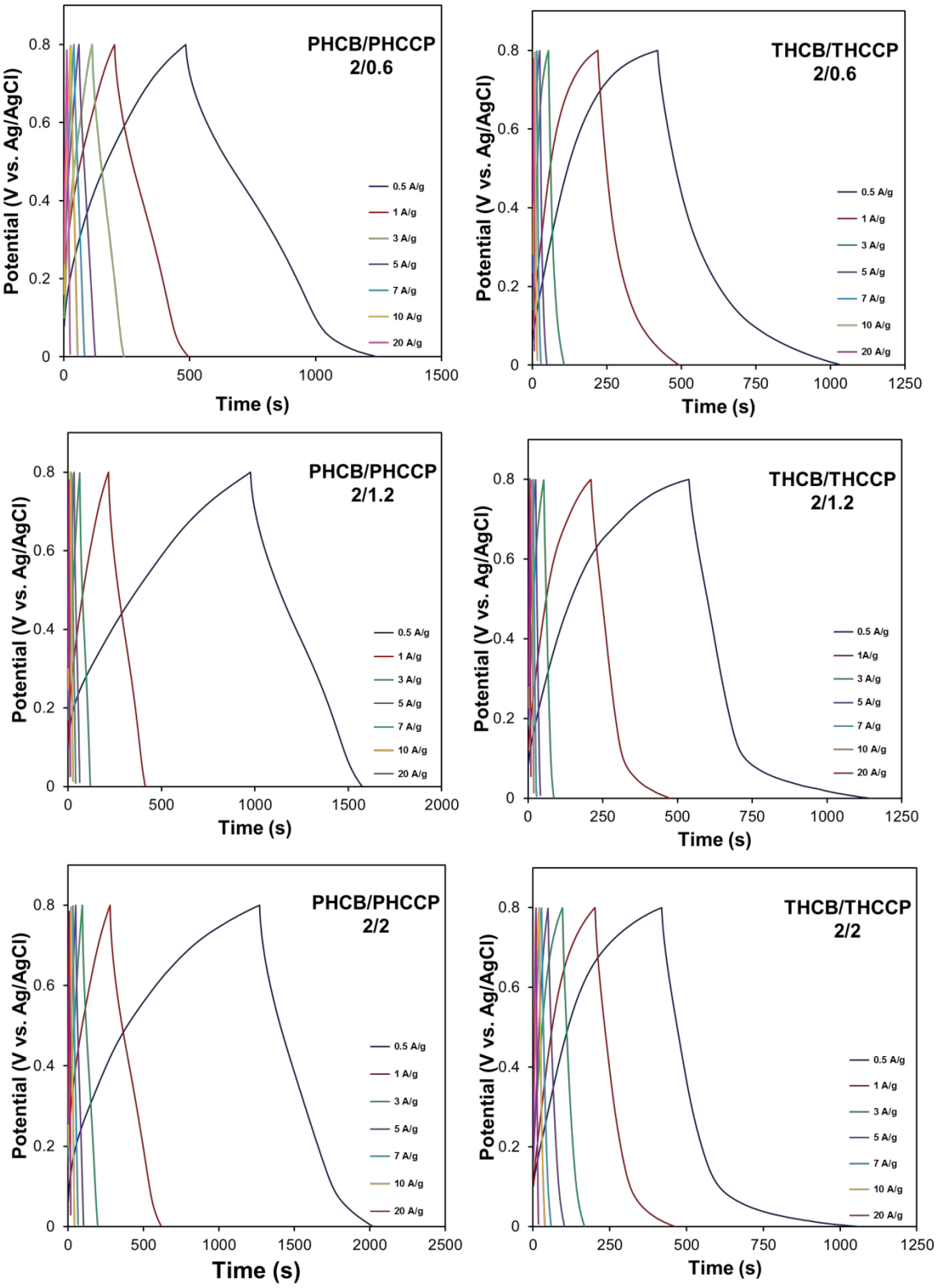


Fig. S14 GCD curves recorded for the carbon films in 1 M Na_2SO_4 aqueous solution at different current densities (0.5 A g^{-1} to 20 A g^{-1}).

Table S4. The specific capacitances (C_S) of the carbon films estimated based on the results of CV and GCD measurements.

sample	C_S (F g^{-1})													
	$C_{S,CV}$ (different scan rates, mV s^{-1})							$C_{S,GCD}$ (different current density, A g^{-1})						
	20	50	100	200	300	400	500	0.5	1	3	5	7	10	20
PHCB	147.6	132.6	110.7	90.3	75.4	68.9	68.8	175.3	146.4	110.9	86.5	70.0	64.4	60.0
THCB	88.1	84.3	80.2	75.8	72.1	70.8	68.1	73.2	52.5	44.8	43.8	36.8	32.8	27.9
PHCCP	277.9	228.7	209.3	184.4	177.3	170.2	167.4	331.8	242.1	178.4	155.3	138.9	129.6	107.5
THCCP	220.6	215.1	196.6	175.3	165.4	160.8	155.9	251.8	206.4	174.5	150.4	135.5	123.3	104.1
PHCB/PHCCP (2/0.6)	157.3	140.2	120.6	105.7	95.9	90.2	87.7	182.0	175.5	100.5	81.6	74.9	65.8	52.7
THCB/THCCP (2/0.6)	102.2	86.1	81.3	67.4	55.2	51.7	49.5	192.8	171.3	93.1	75.0	61.3	50.0	31.5
PHCB/PHCCP (2/1.2)	221.1	195.0	172.9	140.8	127.4	116.4	108.5	186.9	144.4	106.8	93.7	87.5	81.2	70.0
THCB/THCCP (2/1.2)	197.5	152.5	128.9	104.6	94.6	85.1	82.3	191.3	165.6	128.8	104.3	80.0	70.8	60.5
PHCB/PHCCP (2/2)	305.9	247.3	218.1	198.3	183.9	174.5	172.0	235.0	215.5	180.7	162.8	147.0	134.7	110.7
THCB/THCCP (2/2)	306.1	274.3	251.0	218.6	202.2	193.1	185.6	201.4	178.3	156.5	133.1	129.6	115.8	93.6

Table S5. The fit values for circuit elements estimated based on the EIS measurements

sample	R_s (Ω)	R_{ct} (Ω)	Z_W (Ω)	C_{dl} (F)	τ (ms)
PHCB	11.6	181.1	0.0015	43.2×10^{-6}	3.0
THCB	7.5	73.2	0.0051	17.6×10^{-6}	8.8
PHCCP	6.1	340.5	0.0045	79.8×10^{-6}	2.5
THCCP	7.7	364.8	0.0022	152.8×10^{-6}	8.1
PHCB/PHCCP (2/0.6)	5.2	120.6	0.06	663.6×10^{-6}	30
THCB/THCCP (2/0.6)	4.4	65.4	0.01	454.1×10^{-6}	20
PHCB/PHCCP (2/1.2)	6.6	400.2	0.05	732.2×10^{-6}	40
THCB/THCCP (2/1.2)	6.4	290.7	0.08	203.9×10^{-6}	10
PHCB/PHCCP (2/2)	7.1	137.4	0.01	577.4×10^{-6}	40
THCB/THCCP (2/2)	8.6	149.8	0.03	246.7×10^{-6}	20

ESI7. Surface Area and Porosity Characteristics of Carbon films

Table S6. Surface area and porosity characteristics of carbon films

sample	BET specific surface area ($m^2 g^{-1}$)	total pore volume ($cm^3 g^{-1}$)	surface area of pores >1.7 nm ($m^2 g^{-1}$)
PHCB/PHCCP (2/0.6)	1242	1.29	642.7
PHCB/PHCCP (2/1.2)	1454	1.07	560.2
PHCB/PHCCP (2/2)	1955	1.21	935.1

ESI8. References

1 A. A. Ordaz, J. M. Rocha, F. J. A. Aguilar, S. G. Granados, F. Bedioui, *Analusis*, 2000, **28**, 238-244.

2 Z. Kudaş, E. Gür, D. Ekinci, *Langmuir*, 2018, **34**, 7958-7970.

3 A. Isse, S. Gottardello, C. Durante, A. Gennaro, *Phys. Chem. Chem. Phys.* 2008, **10**, 2409-2416.

4 A. Isse, G. Sandonà, C. Durante, A. Gennaro, *Electrochim. Acta*, 2009, **54**, 3235-3243.

5 A. Muthukrishnan, V. Boyarskiy, M. V. Sangaranarayanan, I. Boyarskaya, *J. Phys. Chem. C*, 2012, **116**, 655-664.

6 F. C. Anson, *Anal. Chem.*, 1964, **36**, 932-934.

7 E. T. McBee, R. K. Meyers, C. F. Baranauckas, *J. Am. Chem. Soc.*, 1955, **77**, 86-88.

8 E. T. McBee, D. K. Smith, *J. Am. Chem Soc.*, 1955, **77**, 389-391.

9 E. T. McBee, J. D. Idol Jr., C. W. Roberts, *J. Am. Chem. Soc.*, 1955, **77**, 4375-4379.

10 A. Roedig, L. Hörnig, *Angew. Chem.*, 1955, **67**, 302-300.

11 D. Robb, M. W. Blades, *J. Am. Soc. Mass Spectrom.*, 1997, **8**, 1203-1205.

12 G. A. Tolstikov, S. A. Ismailov, F. A. Gimalova, N. A. Ivanova, M. S. Miftakhov, *Russ. Chem. Bull., Int. Ed.*, 2013, **62**, 226-234.

13 R. S. Pavelyev, R. M. Vafina, O. A. Lodochnikova, A. S. Galiullina, E. I. Romanova, K. V. Balakin, Y. G. Shtyrlin, *Tetrahedron Lett.*, 2016, **57**, 3902-3907.

14 B. V. Lap, M. N. Paddon-Row, *J. Org. Chem.*, 1979, **44**, 4979-4981.